

Continental-scale prediction of hydrologic signatures and processes

Ryoko Araki^{1,2}, Anne Holt¹, John C. Hammond³, Admin Husic⁴, Gemma Coxon⁵, Hilary K. McMillan¹

¹Department of Geography, San Diego State University, San Diego, CA, USA.

²Department of Geography, University of California, Santa Barbara, Santa Barbara, CA, USA.

³U.S. Geological Survey, Maryland–Delaware–DC Water Science Center, Baltimore, MD, USA.

⁴Department of Civil and Environmental Engineering, Virginia Tech, Blacksburg, VA, USA.

⁵School of Geographical Sciences, University of Bristol, Bristol, UK.

Correspondence to: Ryoko Araki (raraki8159@sdsu.edu; raraki@ucsb.edu) and Hilary McMillan (hcmillan@sdsu.edu)

Abstract. Understanding how dominant hydrologic processes and their drivers vary across diverse continental-scale landscapes is critical for hydrologic modeling and water management applications. Our research addresses this question by synthesizing large-sample watershed datasets, Caravan and GAGES-II, and developing random forest models to identify patterns in hydrologic function. We assessed dominant processes by examining hydrologic signatures—summary indicators of watershed function derived from hydroclimatic time series and random forest models across 14,146 gauged United States watersheds. The results reveal clear continental-scale gradients in hydrologic processes, including baseflow, overland flow, storage, and water balance losses. Our map of dominant processes highlights, for example, the transition from baseflow to fast responses and back to baseflow along the elevation gradient from the Appalachian spine, through the Piedmont, to the Eastern Coastal Plain; a distinct outer ring around the Great Lakes region; and sharp contrasts between coastal and inland processes in the West. Variable importance analysis from random forest models show that processes in the western U.S. are primarily controlled by climate, whereas in the eastern U.S., soil, geology, and topography play larger roles, with distinct human influences apparent in urban areas. Our approach of estimating dominant processes and their drivers facilitates extending process knowledge from research watersheds to the continental scale, assessing current hydrological understanding, and evaluating hydrological model structures.

1 Introduction

Estimating the contributions of different hydrologic processes to streamflow generation at a continental scale is essential for flood forecasting and water resources management. Optimal management strategies, including the design of grey and green infrastructure, differ depending on which processes dominate hydrological response (Oswald et al., 2023; Thompson et al., 2020), which vary substantially by regional environmental conditions (Blöschl, 2006; Paola et al., 2006; Penna, 2024). Understanding how water is partitioned, stored, and transported through different parts of the terrestrial systems is a fundamental question in the hydrologic sciences (Brooks et al., 2015). To simulate a diverse set of processes at large-scale, a new generation of hydrologic models with flexible and heterogeneous structures has emerged (Clark et al., 2015; Frame et al., 2025; Johnson et al., 2023). However, despite these technological advances, we still lack an estimate of dominant hydrologic processes controlling streamflow generation at continental scales (McMillan et al., 2025; Reinecke et al., 2025). Developing

34 this understanding is a critical step toward unified hydrologic theory (Sivapalan, 2005) and can provide a blueprint for robust
35 model development and informed decision making.

36

37 Previous efforts to map multiple hydrologic processes at continental scales are scarce. Most large-scale studies have focused
38 on one process. For example, Buchanan et al., (2018) assessed the likelihood of infiltration excess flow occurrence by
39 comparing whether rainfall intensity exceeds saturated hydraulic conductivity, finding that saturation excess dominates across
40 the contiguous United States (U.S.), while infiltration excess is regionally likely in the central U.S. Similarly, studies on
41 baseflow indices have shown their strong dependence on climatic and soil properties (Beck et al., 2013; Xie et al., 2024), and
42 Fang and Shen (2017) quantified the runoff-storage connectivity through correlations between anomalies in streamflow gauge
43 and satellite water storage observations, highlighting large-scale interactions among groundwater table, soil thickness,
44 topography, and snow. In contrast, studies that examined multiple processes have been typically focused on a single or small
45 groups of watersheds. A study in Alaska shows that the use of multiple streamflow statistics can help distinguish and assign
46 hydrologic regions (Barnhart et al., 2022). One of the few studies to holistically investigate storm runoff generation at
47 continental scales (Wu et al., 2021) demonstrates that large-sample analysis aligns with previous conceptual understanding of
48 runoff mechanisms across landscapes (Dunne et al., 1978) while highlighting the roles of precipitation volume and geology.
49 Model-aided studies have simulated global patterns of multiple indices: water partitioning into green and blue water,
50 streamflow response elasticity to rainfall, and streamflow flashiness (Ji et al., 2025), U.S.-wide indices for water balance
51 seasonality (Berghuijs et al., 2014). Another model-based approach has involved inferring hydrologic processes through
52 parameter sensitivity analysis (Hay et al., 2023). These synthesis studies present promising descriptions of spatial patterns and
53 directions for future progress toward a holistic understanding of runoff generation mechanisms, which still remains elusive.

54

55 Much of the research for generalizing watershed function has focused on summarizing flow regimes (Dettinger and Diaz,
56 2000; Lane et al., 2017; Lee et al., 2015; Lins, 1997) and predicting shifts in flow regime under future climate (Brunner et al.,
57 2020; Hodgkins et al., 2024). Many studies cluster streamflow gauges using flow indices that target general (Almagro et al.,
58 2024; Ariano and Ali, 2025; Mosley, 1981; Wu et al., 2021), intermittent (Sauquet et al., 2021), or seasonal streamflow patterns
59 (Dhungel et al., 2016; Haines et al., 1988; Kennard et al., 2010). However, most of these studies aim to define the similarity
60 of flow regimes rather than the underlying runoff generation processes. Furthermore, the results from clustering approaches
61 are constrained to gauged locations and lack spatial coherence, making it challenging to extrapolate to ungauged watersheds.

62

63 To estimate watershed processes in ungauged locations, hydrologists have conventionally used maps derived from
64 physiographic datasets. For example, in the United States context, the Environmental Protection Agency's Ecoregions
65 (Omernik, 1987, 2004), an ecosystem classification based on the physical and biotic characteristics, is a common reference
66 when discussing hydrologic processes (Falcone et al., 2010). Other classifications include the United States Geological
67 Survey's Water Resources Regions (Seaber et al., 1987) based on streamflow networks, Hydrologic Landscape Regions

68 (Santhi et al., 2008; Winter, 2001; Wolock, 2003a) based on physiographic and climatic datasets, and the United States
69 Department of Agriculture's Hydrologic Soil Groups (Web Soil Survey, 2025) based on soil surveys. Nevertheless,
70 regionalization based on physiographic data often fails to capture the full variability of watershed function (Ali et al., 2012;
71 Oudin et al., 2008) because hydrologic processes can differ even among physiographically similar watersheds (McMillan et
72 al., 2014). Capturing watershed processes at a continental scale calls for a scalable method to draw information from
73 hydroclimatic datasets. To date, no studies have attempted to develop comprehensive maps of runoff generation processes
74 based on streamflow observations that can effectively capture watersheds' functions.

75
76 Hydrologic signatures are metrics that quantify hydrologically-relevant dynamics, and offer a promising way to infer watershed
77 processes with minimal data requirements (McMillan, 2021). Hydrologic signature calculations require only widely-available
78 datasets, such as streamflow and precipitation, and can be related to various watershed processes, such as runoff generation
79 and water storage dynamics (McMillan, 2020; Wlostowski et al., 2021). Using hydrologic signatures, expert knowledge, and
80 landscape characteristics, Fenicia and McDonnell (2022) inferred dominant runoff processes and developed perceptual models
81 at the regional scale; and Pechlivanidis and Arheimer (2015) mapped process differences at the national scale in India.
82 Hydrologic signatures can capture the functional streamflow responses to climatic forcings and can discriminate different
83 processes across landscapes (Araki et al., 2022; Gnann et al., 2020, 2021a; Janssen and Ameli, 2021). This enables a signature-
84 based exploration of the relationship between landscape form and function (Bracken et al., 2013; Sivapalan, 2005).

85
86 Watershed attributes describe the physical characteristics of watersheds, which can be used to identify the drivers of hydrologic
87 processes and to transfer hydrological knowledge to ungauged locations (Tarasova et al., 2023). The link between watershed
88 attributes and signatures of streamflow response can be explored via machine learning approaches on large watershed samples.
89 Regional and global applications include studies in the U.S. (Addor et al., 2018; Janssen and Ameli, 2021; Wu et al., 2021),
90 Australia (Trancoso et al., 2017), Zimbabwe (Mazvimavi et al., 2005), Brazil (Almagro et al., 2024), Europe (Rudlang et al.,
91 2025; Kuentz et al., 2017), and globally (Beck et al., 2015). Across all studies, climate emerged as the primary control on
92 signatures. Non-climatic factors (i.e., landscape attributes), such as soil, geology, vegetation cover, and topography, had weak
93 or limited predictive power. However, substantial evidence from field-based studies shows that landscape forms are a primary
94 control of watershed function (Angermann et al., 2017; Fan et al., 2019; Jackisch et al., 2017; Jefferson et al., 2010; Lohse and
95 Dietrich, 2005; Pfister et al., 2017; Zimmer and Gannon, 2018).

96
97 Weak predictive power of non-climatic drivers can be attributed to lack of high-resolution, accurate landscape attributes that
98 describe regionally important processes (Gnann et al., 2021a; Tarasova et al., 2023). For example, wetlands are key regulators
99 of low flows in the U.S. (Worland et al., 2018) and have been left out of previous studies (Addor et al., 2018). Similarly,
100 weathering and glaciation have primary impacts on baseflow storage and generation (Neff et al., 2005; Tague and Grant, 2004),
101 but rock permeability and porosity predictors did not clearly capture the relationship (Wu et al., 2021). Coarse spatial resolution,

102 or limited quality and consistency of global datasets may reduce their predictive power (Nascimento et al., 2025; Beck et al.,
103 2015). Additionally, large-sample studies across broad climatic gradients may be obscuring the influences of landscape
104 attributes. Regional analysis can mitigate this effect and elucidate the non-climatic drivers; for example, regional random forest
105 models have revealed physiographic and anthropogenic controls on flow regimes (Almagro et al., 2024; Hammond et al.,
106 2021). However, smaller regional sample sizes may limit prediction accuracy if datasets only provide tens of watersheds per
107 region (Willard et al., 2024).

108
109 Lastly, the quality of signatures can compromise data-driven model performance and interpretation for process understanding.
110 Examples include the sensitivity of flow duration curve slope to measurement errors (McMillan et al., 2017), the sensitivity of
111 signatures to rating curve uncertainties (Westerberg et al., 2016), lack of process representativeness (McMillan et al., 2022),
112 and inaccurate parameterization of storm separation algorithms (McMillan et al., 2023). Minimizing the impact of signature
113 uncertainty is important for differentiating different regional watershed functionalities (Westerberg et al., 2016).

114 This study presents the first hydrologic processes map for the contiguous United States (CONUS). We synthesized hydrologic
115 signatures as process indicators, going beyond pattern identification from single signatures. We hypothesize that signature
116 combinations can represent six key hydrologic processes (McMillan, 2020; McMillan et al., 2022): baseflow and storage,
117 water balance and seasonal flow variability, and saturation and infiltration excess overland flow. Using random forest models,
118 we demonstrate the explanatory power of landscape metrics to predict hydrologic signatures and their regional variations, and
119 thus the underlying processes, across CONUS.

120
121 We address the limitations of previous studies in predicting hydrologic signatures. First, we improved the quality of non-
122 climatic attributes by: (i) incorporating new geological and wetland landscape attributes that have demonstrated strong
123 connections to baseflow processes (Holt and McMillan, 2025); and (ii) utilizing watershed attributes from GAGES-II datasets
124 (Falcone, 2011), derived from survey-based and higher-resolution products. Second, we interpret random forests using Shapley
125 values (Shapley, 1953) following Husic et al. (2025), as well as permutation importance values within a regional model-
126 building approach, following Hammond et al. (2021), which extends prior work to elucidate the regional contributions of non-
127 climatic, landscape attributes to hydrologic processes. Furthermore, our work assessed 14,146 U.S. watersheds and was trained
128 on 10,261 watersheds, nearly ten times more sample watersheds than previous studies; we leverage the Caravan and GAGES-
129 II—the most extensive open-source large-sample datasets currently available (Falcone, 2011; Kratzert et al., 2023). Third, we
130 utilize a set of hydrologic signatures proven robust across large-sample watershed studies and have a clear connection to
131 critical-zone processes (McMillan et al., 2022), with their parameters further tuned to local storm characteristics. With these
132 improvements, we expand watershed coverage and uncover more detailed spatial patterns of watershed processes than
133 previously possible, using widely-available hydroclimatic datasets and physiographic attributes.

134 **2 Data**

135 We used two primary sources of streamgages and watershed attribute data to expand the number of samples: Caravan v1.5
136 (Kratzert et al., 2023, 2024) and U.S. Geological Survey GAGES-II (Falcone, 2011; Falcone et al., 2010). See Fig. 1 for the
137 spatial distribution of the study watersheds. Caravan is an open-source dataset of global watersheds; its CONUS subset consists
138 of 9,234 watersheds sourced from CAMELS-US (Addor et al., 2017) and HYSETS (Arsenault et al., 2020). GAGES-II is a
139 geospatial dataset of 9,067 watersheds in the United States, selected for their quality to characterize natural and altered flow
140 regimes.

141 **2.1 Hydroclimatic dataset**

142 We calculated hydrologic signatures listed in Table 1 using daily hydroclimatic timeseries data from watersheds within the
143 contiguous United States (CONUS). For Caravan watersheds, we used U.S. Geological Survey (USGS) streamflow
144 measurements paired with daily ERA5-Land forcings provided. For the GAGES-II watersheds, we obtained the USGS
145 streamflow records (U.S. Geological Survey, 2025) using the dataRetrieval package (DeCicco et al., 2018) and gridMET
146 forcings from Wieczorek et al. (2023). For calculating infiltration excess overland flow signatures of Wu et al. (2021;
147 “*RC_Pint*”), we used the hourly precipitation from the North American Land Data Assimilation System 2 (NLDAS-2; Xia et
148 al., 2012) provided through CAMELSH: a Large-Sample Hourly Hydrometeorological Dataset and Attributes at Watershed-
149 Scale for CONUS (Tran, 2025; Tran et al., 2025).

150 **2.2 Watershed attributes**

151 We combined watershed attributes from three sources: (1) Caravan, (2) GAGES-II, and (3) geologic age and wetland attributes
152 (Holt and McMillan, 2025). We added average geologic age and isolated wetland fraction metrics because of their strong link
153 to baseflow processes, which were missing from previous large-sample analyses (Holt and McMillan, 2025). From the Caravan
154 and Holt & McMillan (2025) attribute sets, we excluded binary or categorical attributes, monthly climate variables,
155 uninformative attributes for the CONUS context (e.g., permafrost extent, gross domestic product), and highly correlated
156 attributes (Spearman's $\rho > 0.8$ or < -0.8 ; see Text S1). Where available, Caravan attributes were substituted with GAGES-II
157 attributes, as described in Section 3.2 and Table S1. Table 2 lists the 23 attributes used in the random forest analysis. The
158 purpose of merging Caravan and GAGES-II dataset is to maximize the sample size of watersheds and better capture regional
159 hydrologic variability (see Table S1 and an associated Venn diagram of watershed coverage across datasets).

160 **3 Method**

161 We analyzed 14,146 gauged U.S. watersheds; our map of processes was based on observational data from 10,261 gauged sites
162 and extended using random forest predictions to an additional 3,885 watersheds. See Table S1 and associated figures for an
163 overview of the datasets used and the workflow.

164 **3.1 Calculating hydrologic signatures**

165 A total of 12 signatures (four baseflow and groundwater signatures, four water balance and seasonality-related signatures, and
166 four overland flow signatures) were used to characterize hydrologic dynamics (see Table 1). The signatures were selected
167 based on their reliability in representing processes (McMillan et al., 2022). We calculated signatures using the TOSSH toolbox
168 (Gnann et al., 2021b) and tuned the parameters for event separation for each hydroclimatic region (see Tables S2, S3).

169
170 We filtered out watersheds from our signature calculations based on quality criteria for watershed area and snow used by
171 previous studies, and on the timeseries length needed for signatures to stabilize. First, we removed watersheds from our analysis
172 with uncertain topographic boundaries, showing high discrepancies (>25%) in the estimated drainage area between GAGES-
173 II and Caravan datasets. Errors of <20% are possible due to differences in watershed delineation tools or missing small
174 tributaries (Ray, 2018). Second, for overland flow signature analysis, we excluded snow-dominated watersheds (>20% snow
175 fraction of total precipitation; a >30% criterion were used in McMillan et al., 2022 and Wu et al., 2021); this is because our
176 overland flow signatures can be heavily influenced by periods with no flow response due to snow or frozen conditions. Third,
177 we excluded watersheds with less than 5 years of streamflow observation record, and those with over 30% missing daily data
178 over the period where streamflow was recorded (yielding at least three years of available data). Studies suggest that temporal
179 hydrologic variability is adequately captured with 3 to 5 years of data (Refsgaard and Storm, 1996; Klemeš, 1986; Merz et al.,
180 2009).

181 **3.2 Training random forest models and predicting hydrologic signatures**

182 We developed random forest models to examine potential drivers of hydrologic processes. Random forest models have been
183 widely used for this task (Eng and Wolock, 2022; Lapides et al., 2023; Zipper et al., 2021) for their interpretability, relatively
184 low computational demands, and robustness to multi-collinearity (Addor et al., 2018). For each signature, we constructed a
185 random forest model to predict its values based on watershed attributes using the caret R package (Kuhn, 2008; R Core Team,
186 2024). Each model used 500 trees with the optimal number of features randomly resampled at each split, selected by
187 minimizing root mean squared error (RMSE) through 10-fold cross-validation.

188
189 Only the signatures calculated from quality-controlled streamflow records (as described in Section 3.1) were used for training.
190 Training on all Caravan watersheds yielded $R^2 < 0.4$ for many of the signatures, so we limited the training samples to the 4,748
191 Caravan watersheds with streamflow gauge IDs overlapping with GAGES-II to attain model performance comparable to
192 previous studies (see Text S2). When a gauged watershed was present in both datasets, we prioritized CAMELS over HYSETS,
193 and Caravan over GAGES-II. This is to ensure the broader applicability of our method across different countries, as Caravan
194 is available at global scale. This yielded a total 14,146 watersheds for signature analysis (overview in Table S1).

195

196 We then used the trained model to predict hydrologic signatures for 3,885 watersheds where observations did not meet data
197 quality standards as described in Section 3.1. Previous study (do Nascimento et al., 2025) and our preliminary experiments
198 (Text S2) showed improved model performance when the watershed attributes were derived from higher-resolution datasets
199 based on detailed field surveys, such as in GAGES-II and Holt and McMillan, (2025). Therefore, we used GAGES-II attributes
200 and when unavailable, used the coarser resolution Caravan attributes (see Table S1).

201 **3.3 Interpretation of hydrologic signatures as process descriptors**

202 We combined signatures calculated from observed streamflow data and predicted with random forest models to develop a
203 comprehensive map of processes for watersheds across the U.S. (Fig. 1). A bivariate space of hydrologic signatures was used
204 to infer process dominance. For each selected process, we used the two signatures most strongly related to the process inferred
205 from previous work (Bolotin and McMillan, 2024; McMillan, 2020; McMillan et al., 2022; Wu et al., 2021). Each signature
206 was categorized based on the quantiles of signatures, from low (0-25%), mid-low (25-50%), mid-high (50-75%), to high (75-
207 100%). When both of the two target signatures had mid-high (50-75%) or high (75-100%) values, we interpreted this as
208 indicative of process dominance. This bivariate matrix can highlight the complexity of hydrologic processes where two
209 signatures do not necessarily show the same trends.

210

211 The process hypotheses tested are described in Table 1 and cover six major hydrologic processes: baseflow, watershed storage,
212 water balance, seasonal variability, overland flow dominance, and its type. Baseflow sustains discharge across seasons and
213 reflects groundwater connectivity, while overland flow drives stormflow and influences flood peaks. Storage governs buffering
214 and recession dynamics, and water balance losses through evapotranspiration and deep percolation determine how much
215 precipitation is converted to streamflow. Together, these processes span the continuum from slow to fast hydrologic response
216 and integrate both vertical and lateral fluxes, making them essential for hydrologic theory and modelling (Bergström, 1992;
217 Kirchner et al., 2009; Berghuijs et al., 2014).

218 **3.4 Interpretation of process drivers using Shapley values**

219 We quantified feature importance using Shapley values (Shapley, 1953), which provide a robust and consistent measure to
220 interpret random forest models (Lundberg et al., 2018). Shapley values represent the average marginal contribution of a feature
221 (i.e., a landscape attribute) to a prediction, given the effects from all combinations of the considered features. Shapley values
222 allow for local and global interpretation of machine learning model predictions, helping to uncover site-specific and
223 generalizable linkages between hydrology and landscape features (Husic et al., 2025). We used the interpretable machine
224 learning (iml) R package (Molnar et al., 2018) to calculate Shapley values over the training data.

225

226 To evaluate the regional effects of watershed attributes, we computed summary statistics on Shapley values. Shapley values
 227 are site-specific: $\phi_x^{(y,i)}$ is the Shapley value calculated for an attribute x for a signature y at location i . Summing the Shapley
 228 values across watershed attributes x at a single location gives the deviation of the predicted signature value y_i at location i from
 229 the mean signature value across all sites. To compare effects of a landscape attribute x across sites, we normalize Shapley
 230 values by the total absolute contribution from all attributes at a site i ; this gives a metric for the relative contribution of an
 231 attribute x to signature y at site i as:

$$232 \quad R_x^{(y,i)} = |\phi_x^{(y,i)}| / \sum_{x \in A} |\phi_x^{(y,i)}|$$

233 where A is the set of all watershed attributes, and $|\cdot|$ denotes the absolute value. To investigate which types of landscape
 234 characteristics are influential, we classified the watershed attributes into five categories (see Table 2), namely, topography,
 235 land-cover, soil & geology, human alteration, and climate.

236
 237 Then, the average relative contribution of category k for signature y at location i , $\bar{R}_k^{(y,i)}$, is calculated as:

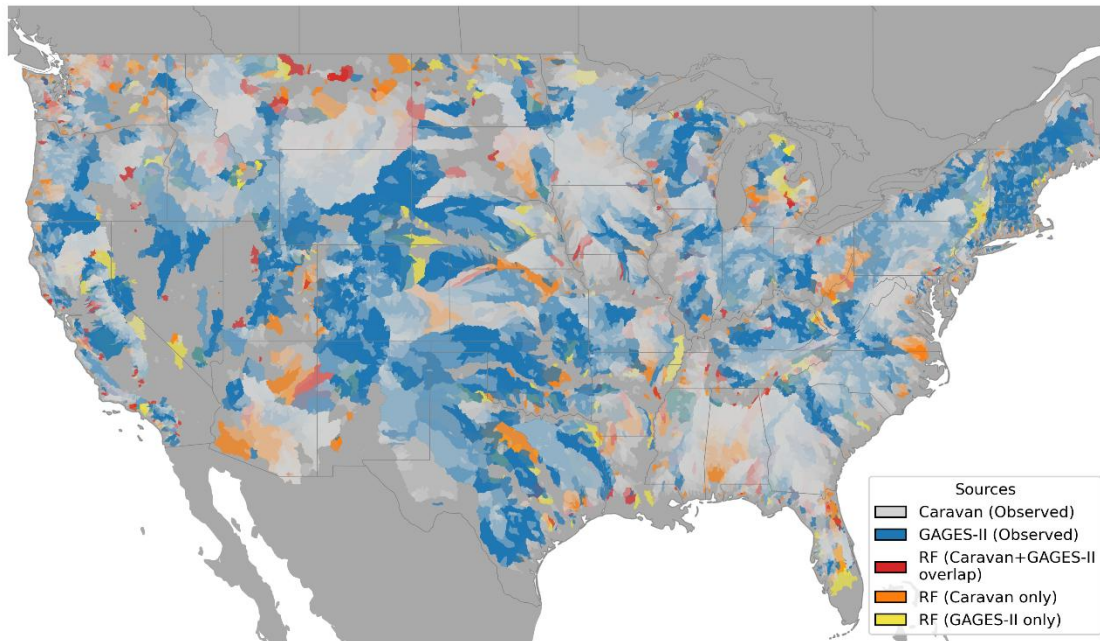
$$238 \quad \bar{R}_k^{(y,i)} = \frac{1}{K} \sum_{x \in C_k} R_x^{(y,i)}$$

239 , where C_k is the set of watershed attributes belonging to category k , and K is the number of categories (in our case, five).

240 **3.5 Interpretation of process drivers using permutation importance**

241 To further evaluate locally important watershed attributes, we computed permutation importance, which measures the change
 242 in model performance when a feature (i.e., a landscape attribute) is removed. Prior work has shown that permutation
 243 importance derived from random forest models trained on regional samples is more effective than a continental approach for
 244 identifying physiographic, landscape controls on hydrologic responses, as it allows assessment under consistent climate
 245 conditions (Almagro et al., 2024; Hammond et al., 2021; Holt and McMillan, 2025). Therefore, we calculated permutation
 246 importance as the average changes in mean squared error (MSE), normalized by its standard deviation using the caret R
 247 package (Kuhn, 2008), from random forest models trained on regional watershed samples. Six climate regions were defined
 248 using a Gaussian mixture model in Scikit-learn (Pedregosa et al., 2011) based on relevant Caravan, GAGES-II, and Hammond
 249 et al. (2023) climate attributes (Table S4), and separate random forest models were trained for each region. Fig. S1 shows the
 250 identified climate regions.

251



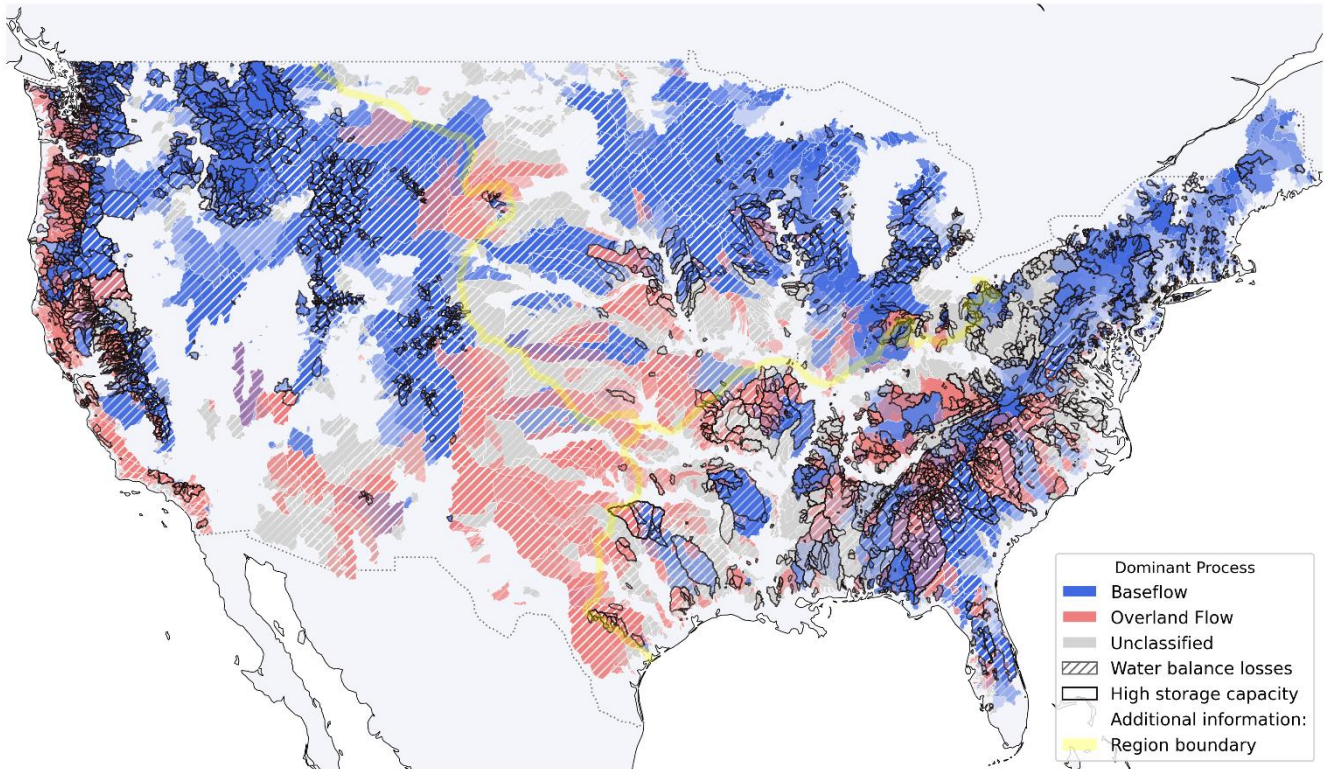
252

253 **Figure 1: Method used to obtain hydrologic signatures. Signatures are derived either from observed data (“Observed”: Caravan**
 254 **samples, n=7,465; GAGES-II samples, n=2,807; total n=10,261) or predicted using random forest models (“RF”; n=3,885). Predicted**
 255 **samples are categorized as: “Caravan+GAGES-II overlap” (present in both the Caravan and GAGES-II datasets; n=618), “Caravan**
 256 **only” (exclusive to Caravan; n=2,424), and “GAGES-II only” (exclusive to GAGES-II; n=843). State boundaries are indicated by**
 257 **grey lines.**

258 **4 Results**

259 **4.1 Mapping dominant processes across the contiguous U.S.**

260 Figures 2 and 3 show the maps of dominant processes derived from the hypotheses outlined in Table 1. Figure 2 presents the
 261 signature of each process hypothesis in a bivariate map. Figure 3 provides a summary, displaying the four primary hydrologic
 262 processes when it is deemed dominant (i.e. both signatures are in the mid-high (50-75 %) or high (75-100 %) quantiles).
 263 Together, these maps highlight distinct regional patterns in hydrologic processes across the study area. The following sections
 264 examine these patterns in greater detail by region: the East and South. (Section 4.2.1.), the Midwest and Central (Section 4.2.2.),
 265 and the West and Southwest (Section 4.2.3.).



266

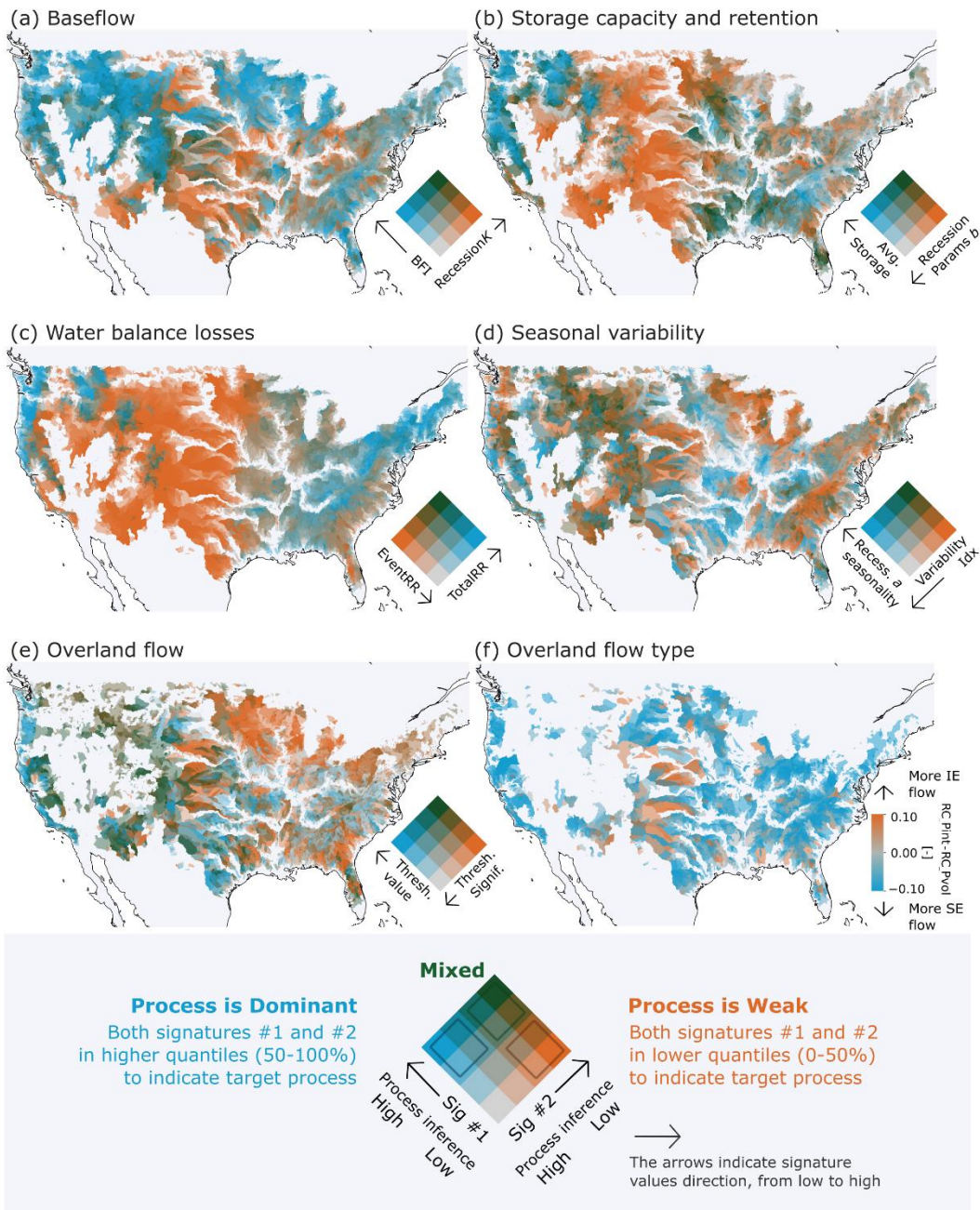
267

268

269

270

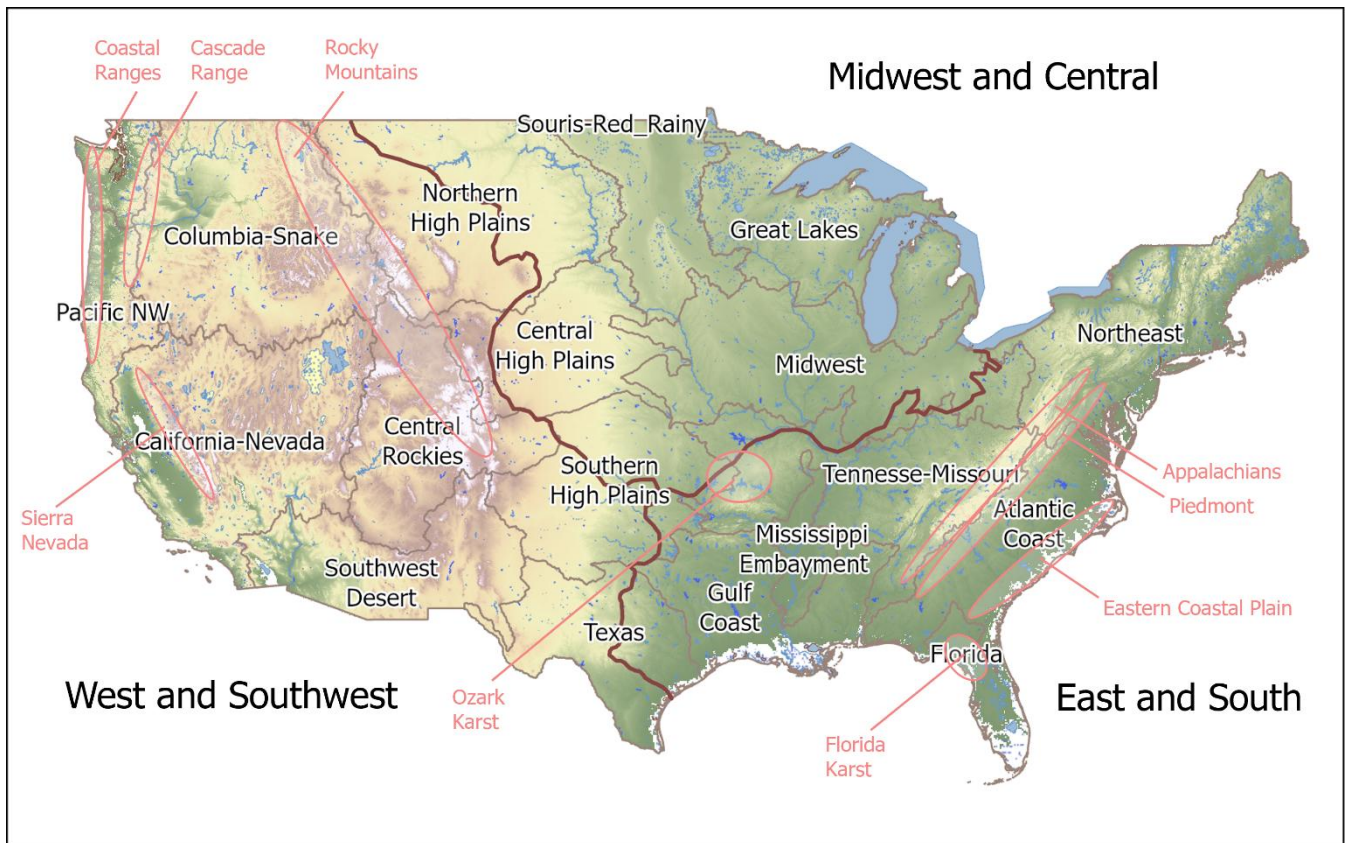
Figure 2: Map of dominant processes estimated based on our hypothesis (defined in Table 1 and Section 3.3). Note that when baseflow and overland flow both occur, their colors are overlaid to give purple hues. “Unclassified” means a watershed is deemed neither baseflow- nor overland-low-dominant. “Region boundary” indicates the areas described in Section 4.2.1-4.2.3 (East and South (bottom right), Midwest and Central, West and Southwest (left in the figure)).



271

272

273 **Figure 3: Hydrologic signatures of each process hypothesis, shown in bivariate maps (a–e). See the legend at the bottom for**
 274 **explanation. The high-process quantile from (a) is used to infer “Baseflow” in Figure 2; from (b) to infer “High storage capacity”;**
 275 **from (c) to infer “Water balance losses”; and from (e) to infer “Overland flow.” Panel (f) shows the differences between the two**
 276 **signatures related to infiltration-excess (IE) flow and saturation-excess (SE) flow (i.e., values of *IE Correlation* (*RC_{Pint}*) minus *SE***
 277 ***Correlation* (*PC_{Pvol}*)). In the overland flow panels (e) and (f), watersheds dominated by snow (i.e., where more than 20% of annual**
 278 **total precipitation falls as snow) are not shown. For the overland flow type pane (f), watersheds are not shown when the correlations**
 279 **between the event runoff coefficient and both rainfall characteristics (i.e., storm rainfall volume and maximum intensity) are**
negative. For maps of each signature value, see Figures S2 and S3. See Table 1 for signature names’ abbreviations.



280

281 **Figure 4: Map of the contiguous United States showing (i) areas described in Section 4.2.1-4.2.3 (East and South, Midwest and**
 282 **Central, West and Southwest; bolded brown line) (ii) geographical boundaries used for the USGS National Water Availability**
 283 **Assessment (Qi and Mason, 2023; Stets et al., 2025; Van Metre et al., 2020) (beige line) (iii) topographic and geological features**
 284 **named in the text (pink annotations).**

285 **4.2 Spatial patterns of hydrologic processes inferred from signatures**

286 **4.2.1 Region 1: East and South**

287 This humid region has moderate to high precipitation (1,000-1,500 mm/yr; calculated based on the 10th and 90th percentiles
 288 of sample watershed attributes), with low precipitation seasonality except in Florida. Temperatures vary widely from snow-
 289 dominated areas in the NorthEast to subtropical areas in Florida, with mean annual temperature ranging from 7-19°C (Fig. S4).
 290 The landscape is old with deeply weathered soils and characterized by predominantly low-lying elevation (mean watershed
 291 elevation ranges between 40-600m), though there is a primary elevation gradient from the Appalachian Mountains and
 292 Piedmont to the Eastern coastal plains, with peaks exceeding 1,000m (Fig. S8). In Figure 3, signature values show that these
 293 climate and landscape conditions produce slowly-varying, baseflow-dominated flow regimes and mid-quantile signature
 294 values showing a lack of hydrologic extremes. Runoff ratios (*Total Runoff Ratio and Event Runoff Ratio*; Fig. 3c) are moderate
 295 or high and seasonal variability in flow and recessions is moderate to low. Storage capacity (*Average Storage*) is overall

296 moderate, but recession shapes (*Recession Parameter b*) are variable (Fig. 3b). Evidence for overland flow is weak with
297 saturation excess prevailing when it occurs (Fig. 3e,f).

298

299 The gradient along the geographical transect from the Appalachian spine to the Eastern coastal plain is apparent in several
300 processes. The Appalachians have strong baseflow influence, shown by high baseflow index and slow recessions (Fig. 3a).
301 Nonlinear recessions (high *Recession Parameter b*; Fig. 3b) indicate multiple groundwater reservoirs supplying baseflow. In
302 contrast, the Piedmont has lower baseflows and fast recessions, relating to lower storage. The Eastern coastal plain, especially
303 towards the South, has high baseflow and moderate to slow recessions (Fig. 3a). Linear recessions suggest a single dominant
304 groundwater reservoir supplying baseflow in this sandy, coastal plain aquifer (Fig. 3b). Lower runoff ratios in the coastal plains
305 indicate losses to deep groundwater including offshore discharge, especially in Florida's karst area (Fig. 3c, S6). The karst
306 area stands out for its high dynamic storage and seasonality in recessions. Saturation excess dominates overland flow in the
307 Coastal plain (Fig. 3f), although evidence for overland flow is weak (Fig. 3e) in contrast to a previous study (Wieczorek and
308 LaMotte, 2010) that suggests the Florida panhandle has the highest fraction of saturation excess overland flow in the US.

309

310 In inland areas such as the valleys of the Tennessee-Missouri region, baseflow is moderate and recessions are relatively fast
311 (Fig. 3a). The Gulf Coast region has lower baseflow and faster, linear recessions. Infiltration excess flow largely occurs in the
312 narrow ocean margin of the Gulf Coast region but does not extend far inland (Fig. 3f). Exceptions to the area's fast runoff
313 occur in the Ozark Mountains and the west of the Mississippi embayment where limited areas of high baseflow and slow
314 recessions occur.

315 **4.2.2 Region 2: MidWest and Central**

316 The landscape of the Midwest and Central region is dominated by the gradient from recently-glaciated, sandy, forested
317 watersheds of the Great Lakes region, to the poorly-drained, clay-rich but highly developed for agriculture and populated
318 region of the Souris-Red-Rainy and Midwest regions. Across the Midwest and Central area, mean watershed elevation ranges
319 from 200 to 700 meters, and mean annual precipitation varies from 500 to 1,000 mm. Moving west into the Central and
320 Northern High Plain regions, elevation gradually increases, precipitation decreases, and population density decreases (Fig. S8,
321 S4, S7). The region experiences mean annual temperatures between 6 to 13°C. The absence of major topographic barriers
322 results in a continental climate characterized by intense thunderstorms in summer and heavy snowfall in winter.

323

324 Signature values show that storage capacity is moderate throughout the Midwest (Fig. 3b). Storage in this region is provided
325 by a moderate snowpack and high depth to bedrock (Fig. S5). Most of the region was previously glaciated, leaving a thick
326 layer of glacial drift. The soil texture is graded from coarse and sandy around the Great Lakes to clay-rich further South and
327 West, forming a distinctive outer ring around the Great Lakes region (Miller and White, 1998; Fig. S6). Following this gradient,
328 there is no significant evidence for overland flow around the Great Lakes, changing to stronger evidence further South-West

329 (Fig. 3e,f). Some occurrence of infiltration excess is consistent with evidence of this process from Midwest agricultural
330 watersheds (Abban et al., 2014; Davis et al., 2014; Wilson et al., 2012). Streamflow seasonality follows the same gradient (Fig.
331 3d), with low seasonality around the Great Lakes where sandy aquifers sustain discharge year-round, and higher seasonality
332 further SouthWest (Miller and White, 1998; Fig. 3d). A second gradient occurs in the MidWest from West to East, following
333 precipitation and aridity gradients (Fig. S4). In the west, high aridity leads to high water balance losses to ET and low runoff
334 coefficients at the annual and event scale (Fig. 3c).

335 **4.2.3 Region 3: West and Southwest**

336 The landscape of the West and Southwest region is dominated by the mountain ranges of the Coastal Ranges, Cascades, Sierra
337 Nevada and Rocky Mountains, with mean watershed elevation ranging from 400 to over 2,700 meters. Dense populations in
338 the coastal cities give way to sparsely populated inland areas. The climate exhibits strong gradients. The Pacific Northwest
339 and Sierra Nevada mountain ranges receive substantial amount of precipitation than interior, with mean annual precipitation
340 ranging from 460 to over 2,100 mm/yr across the region. The region shows a north-south temperature gradient with coastal
341 moderation. Mean annual temperature ranges from 2°C in northern and high mountain areas to over 20°C in inland southern
342 desert regions (Fig. S4). Precipitation patterns follow Mediterranean or semi-arid climates characterized by winter precipitation
343 peaks and dry summers.

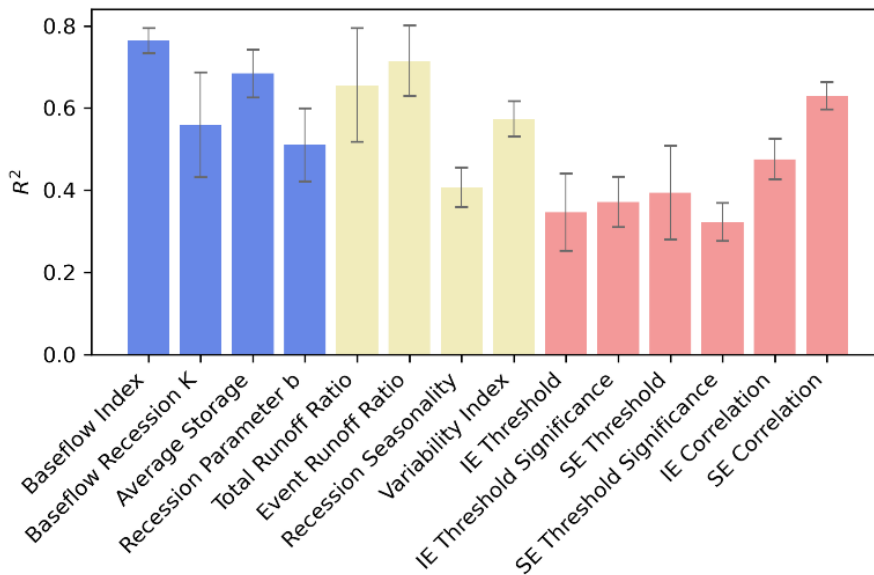
344
345 High baseflows with slow recession are prevalent across most of the Western region, where deep snowpacks drive sustained
346 baseflow processes (Fig. 3a, S5; Barnhart et al., 2016; Tague and Grant, 2009). Inland areas tend to have faster recessions
347 while retaining high baseflows, while coastal areas - where snow is rare - have lower baseflow while retaining slow recessions.
348 The Southwest desert contrasts with the rest of the region, having low baseflows and fast recessions typical of the arid or semi-
349 arid climate with water tables far below the land surface (Goodrich et al., 1997). Storage capacity and retention follow the
350 same gradient from high in the Pacific Northwest to low in the South-East, but the high storage region is more constrained to
351 the Rocky, Cascade and Sierra Nevada mountains (Fig. 3b). Water balance patterns contrast the pattern still further, with only
352 the high mountains having high runoff ratios in contrast to low ratios throughout the remainder of the Western U.S. (Fig. 3c)
353 Seasonal variability in processes is higher in the South (primarily California) where the seasonal Mediterranean climate pattern
354 occurs with hot, dry summers and cool, wet winters (Fig. 3d, S5).

355
356 Processes in the coastal margin are markedly different from those inland. The moderating influence of the coast is strongly
357 apparent in storage capacity (Fig. 3b): the northern Coast Ranges have lower average storage compared to high storage inland
358 areas, while the southern coastal band has higher storage compared to low storage inland areas. Overland flows are strongly
359 indicated all along the coast, but more weakly inland (Fig. 3e). Most overland flow favors saturation excess, although inland
360 watersheds of the Southwest desert show areas of infiltration excess (Fig. 3f).

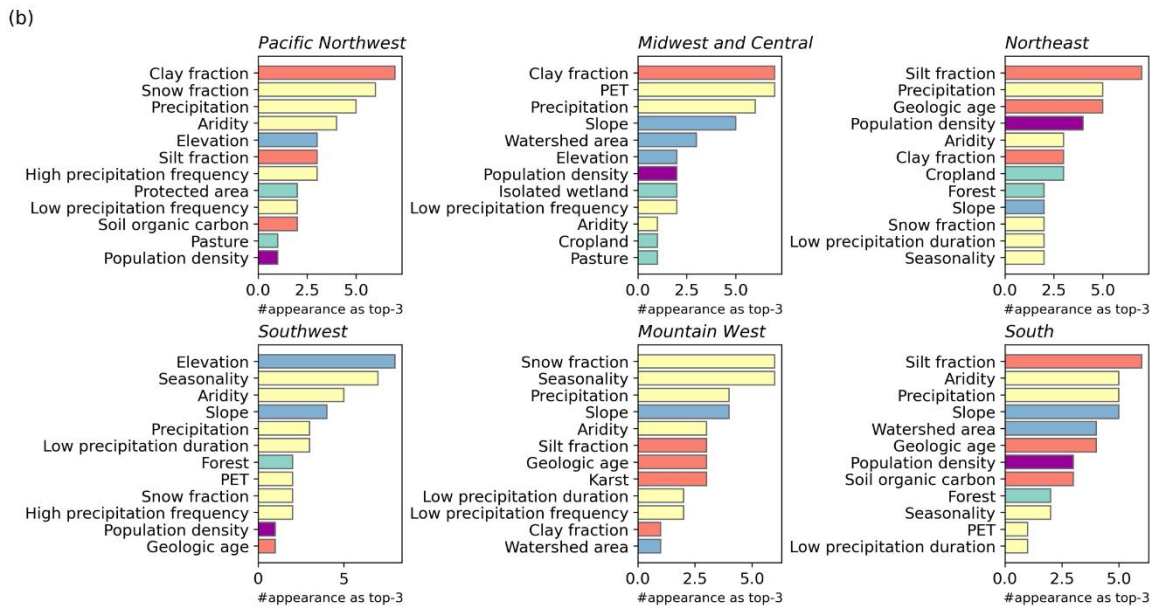
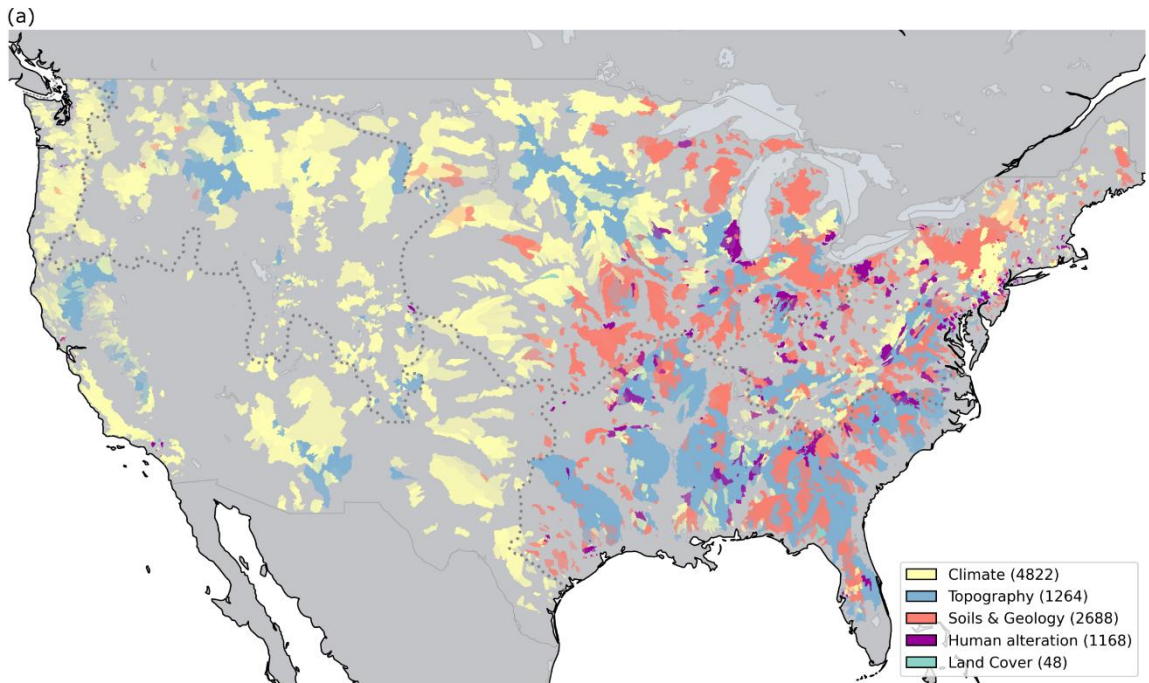
361 4.3 Inferred climate and landscape drivers of hydrologic processes

362 In this section, we interpret the random forest models to understand which aspects of climate and landscape are most important
363 in controlling hydrologic processes in different regions of the U.S. We hypothesize that variable importance statistics from
364 Shapley and permutation analysis reflect the relative importance of hydrologic process drivers. Random forest models
365 performed reasonably well ($R^2 > 0.4$) for most signatures (Fig. 5), consistent with previous studies using similar model setups
366 (Addor et al., 2018; Beck et al., 2015; Bolotin and McMillan, 2024; Kuentz et al., 2017). Performance was higher for baseflow,
367 water balance loss, and seasonality signatures, but lower for overland flow signatures. Figure S9 presents the regional model
368 performances for each signature.

369
370 Figure 6 provides an overview of variable importance results: Figure 6a focuses on spatial patterns, showing the landscape
371 attribute category that has the strongest contribution to predictions of signatures and processes for each watershed, calculated
372 using aggregated Shapley values; Figures 6b provides deeper insights into the ranking of landscape attributes, ordered by
373 permutation importance, for predicting signatures in each region. Figure S10 complements Figure 6a by showing the
374 importance of landscape attribute categories in each region, based on permutation importance.



375
376 **Figure 5: Ten-fold cross-validation performance of the random forest model trained on 4,748 CONUS-samples, where gauge IDs**
377 **overlapped with Caravan and GAGES-II. Bars show the average R^2 between observed and predicted signatures, with error bars**
378 **representing the standard deviation. See Table 1 for signature definitions.**



379

380

381

382

383

384

385

386

Figure 6: (a) The landscape attribute category that contributes most to hydrologic responses was identified based on the average relative contribution of each category, $\bar{R}_k^{(y,i)}$ (derived from Shapley values; see Section 3.4). For each watershed, the most important category k was determined using the median of $\bar{R}_k^{(y,i)}$ across all hydrologic signatures. Results are displayed for the watershed samples included in the random forest training. Numbers in the legend indicate the frequency that each category was identified as the most important. (b) Frequency of watershed attributes ranked among the top three most important variables in permutation importance (IncMSE%) across all signatures in six U.S. climate regions. The x-axis indicates how many times each attribute appeared in the top three. See Section 3.4 and Table 2 for attribute names.

387 **4.3.1 Region 1: East and South**

388 In the East and South, a wide variety of landscape attribute categories dominate process predictions, including topography,
389 soils and geology, climate and human alteration (Fig. 6). Climate attributes dominate in cooler areas in the Northeast and along
390 the Appalachian spine, while topography attributes dominate on the Eastern coastal plain. Along the Gulf Coast, either climate
391 or soils and geology may dominate. Human alteration attributes dominate clusters of watersheds around cities including New
392 York, Philadelphia, Washington D.C., Raleigh and Atlanta.

393
394 Overall, and particularly for signatures relating to storage and water balance in the East and South Region (*Total Runoff Ratio*,
395 *Event Runoff Ratio*, *Recession seasonality*, *Average Storage*, *Recession Parameter b*), the random forest models show that
396 climate drivers are less important than in the rest of the U.S., and soils and geology, topography, and land cover drivers are
397 more important (Fig. 6, S10). Human influence (population density) is a more important driver here than in other regions
398 across most signatures, consistent with large areas of high population (Fig. S7). In addition to the major cities, highly developed
399 areas of Western Florida show anomalous areas of low baseflow, as do developed Piedmont areas (Zimmer and Gannon, 2018).

400
401 In the NorthEast, across all signatures, the drivers that most often appeared in the top three controls of random forest
402 performance were Silt fraction, Precipitation, Geologic age and Population density — representing the effects of geology, soils,
403 climate and human development (Fig. 6b). Climate characteristics appear more often for signatures related to water balance
404 and overland flow. In the South, Silt fraction, Aridity, Precipitation and Slope occur most often, representing gradients in
405 elevation and soils from the Appalachians to the coastal plain and into Florida (Fig.s S6, S8).

406 **4.3.2 Region 2: MidWest and Central**

407 In the Midwest and Central area, a wide variety of landscape attribute categories dominate process predictions, including
408 topography, soils and geology, climate and human alteration, showing strong spatial patterns (Fig. 6). Soils and geology
409 attributes dominate in the Great Lakes region, and in the arc of clay-rich soils in the High Plains and Midwest regions (Fig.
410 S6). A mixture of climate and topography attributes dominate in the Souris-Red-Rainy region. Human alteration attributes
411 dominate in clusters of watersheds around Chicago, Detroit and Cleveland.

412
413 Overall in the Midwest and Central area, the random forest models show that land cover and topography drivers are more
414 important than in the rest of the U.S., while climate drivers are less important. Across all signatures, the drivers that most often
415 appeared in the top three controls of random forest performance were Clay fraction, PET, Precipitation and Slope —
416 representing the effects of soils, climate and topography (Fig. 6); this is consistent with the gradual variation in signatures'
417 spatial patterns accompanying gradients in glacial drift and climate in this region, as discussed in 4.2.2. Despite the flat
418 topography of the region, several topographic attributes appear in the top ten, perhaps reflecting the effect of unusual

419 topographic features such as the driftless area. Land cover metrics (wetland, cropland, pasture) were secondary drivers,
420 appearing for signatures related to storage and overland flow.

421

422 The impact of climate is spread between multiple drivers: PET, Precipitation, Low precipitation frequency and Aridity. Climate
423 drivers in the Midwest and Central area show multiple distinct spatial patterns, with aridity and low precipitation metrics
424 showing an east-west gradient, temperature and PET having a north-south gradient, and precipitation and seasonality having
425 a Northwest-Southeast gradient (Fig. S4, S5). Thus, each part of the Midwest and Central area has a unique holistic climate
426 combination. Climate patterns differ distinctly from the NorthEast-Southwest pattern of the soils and land cover.

427 **4.3.3 Region 3: West and Southwest**

428 In the West, climate attributes dominate process predictions across most watersheds in the Pacific Northwest and Mountain
429 West (Fig. 6a, S5). Some mountain areas have dominant topographic attributes, and topography drivers are more important in
430 the Southwest region compared to the wider U.S.. Climate properties that appear most often include Snow fraction,
431 Precipitation, Aridity and Seasonality (Fig. 6b: regions Pacific Northwest, Southwest, Mountain West). These attributes
432 describe the primary climatic features of the West and Southwest U.S., which are governed by precipitation and aridity
433 gradients from North to South, and from coasts to inland (Fig. S4). Inland mountain chains influence flow regimes by providing
434 spring snowmelt and mountain block recharge, among the many influences of topography on hydrologic processes (Gnann et
435 al., 2025). These controls are demonstrated by the importance of snow fraction alongside topographic attributes, elevation and
436 slope. Soil control on runoff process is seen by the importance of clay fraction in the Pacific Northwest, reflecting Oregon's
437 common clay soils (Miller and White, 1998).

438 **5 Discussion**

439 This study creates comprehensive maps of hydrologic processes across the contiguous United States by using machine learning
440 to analyze streamflow signatures and connecting these signatures to dominant watershed processes. The analysis from over
441 10,000 watersheds shows distinct regional patterns in estimated hydrologic processes and its potential drivers. These process
442 maps provide novel information for selecting appropriate hydrologic models across large domains and help hydrologists
443 anticipate how watersheds will respond to environmental changes such as altered climate or land use. In the following sections,
444 we discuss how these maps provide new benchmarks (Section 5.1), inform hydrologic modelling (Section 5.2), and outline
445 directions for future work (Section 5.3).

446 **5.1 New benchmark maps of process understanding over large domains**

447 Our results build on previous work to map hydrologic processes and drivers. Our map of baseflow process importance shows
448 similar patterns to previous studies into baseflow and groundwater contribution to streamflow (Beck et al., 2013; Santhi et al.,

449 2008; Xie et al., 2024). As with those studies, our approach of using observations and machine learning methods provides finer
450 detail than can be estimated using statistical interpolation or by hydrologic or climate models. By combining multiple recent
451 datasets, we increase the number of observations used in our analysis. In our study, we used >10,000 observed watershed data
452 within CONUS, representing a substantial advancement compared to the >600 to >3000 observation samples used in previous
453 studies (Addor et al., 2018; Beck et al., 2013, 2015; Janssen and Ameli, 2021; Wu et al., 2021). Our analysis therefore provides
454 a new benchmark, offering the most comprehensive coverage and highest spatial characterization of hydrologic processes
455 across the contiguous United States to date. While larger datasets have been analyzed elsewhere, for example, >8,000
456 watersheds (Santhi et al., 2008), >23,000 watersheds (Xie et al., 2024), those efforts focused exclusively on baseflow index.
457 Beck et al. (2013) found sometimes differing drivers of baseflow index and recession slope despite their close connection: by
458 using bivariate plots, we could more clearly highlight regions where patterns of these two signatures diverge. Those areas
459 include the Pacific Northwest coast with lower baseflow index but slow recessions, and the central high plains with high
460 baseflow index but fast recessions.

461
462 Previous studies investigated patterns of overland flow generation across the U.S. using soil maps and rainfall intensity
463 (Buchanan et al., 2018) streamflow signatures (Wu et al., 2021) and modeling approaches (Wolock, 2003b). Like us, Buchanan
464 et al. (2018) and Wu et al., (2021) found infiltration excess runoff important throughout the high plains, and saturation excess
465 in the valleys of the Tennessee-Missouri region, and a mixture of saturation and infiltration excess in the Southwestern U.S..
466 Substantial overland flow occurs in Southwest chaparral systems (Valeron and Meixner, 2010), and although deep groundwater
467 tables suggest infiltration excess, we found a mixture of mechanisms. This may reflect vegetation shifting the inferred overland
468 flow mechanism toward saturation excess. Infiltration excess is inferred when overland flow is related to storm intensity rather
469 than storm size. In arid and semi-arid catchments, vegetation can locally increase infiltration capacity and soil water retention,
470 reducing the extent of infiltration excess overland flow (Stein et al., 2021). Additionally, where smaller storms are intercepted
471 by canopies, signatures may incorrectly attribute the runoff to saturation excess rather than infiltration excess. However, our
472 results are supported by global studies that show saturation excess is always more common than infiltration excess even in arid
473 regions, as saturation excess is generated in riparian zones and topographic convergence areas where water tables are higher
474 (McMillan et al., 2025).

475
476 By mapping and categorizing the primary drivers of runoff processes, we can untangle which physical characteristics drive the
477 hydrologic response in each region. In the East and South, soil, geology, and topography emerged as primary drivers, which
478 is consistent with regional hydrologic process knowledge. Topography is important in the Appalachian Piedmont, where wide
479 and wet valley bottoms generate fast responses (Zimmer and Gannon, 2018). Soils are important along the Gulf Coast where
480 clay-rich soils promote infiltration-excess overland flow (Miller, 1999; Fig. S6), producing mixed storage and water balance
481 signatures despite deep bedrock (Fig. S5) and semi-consolidated sand aquifers; and on the Eastern Coastal Plain where sandy
482 soils, seasonal flooding, and wetlands likely support a single dominant groundwater reservoir supplying baseflow (Fig. 3b;

483 Holt and McMillan, 2025; Hupp, 2000). The machine learning approach is especially powerful for this purpose, as multiple
484 landscape attributes often contribute simultaneously to the hydrologic response.

485

486 Our maps of primary drivers based on Shapley values extend previous work to analyze the drivers of hydrologic signatures.
487 For example, Addor et al. (2018; their Fig. 3) show that climate (aridity, seasonality, snow fraction) is the primary driver across
488 most signatures, with topography (elevation, slope) and land cover (forest, leaf area index) being secondary drivers. Figure 6a
489 similarly shows climate and topography as dominant, but adds spatial information to show that, for example, climate is
490 dominant in the mountainous western U.S., but soils and geology dominate the Midwest and much of the Northeastern U.S.
491 Geological age, a recently-proposed attribute to summarize watershed geology, was often in the top random forest attributes
492 (Holt and McMillan, 2025). This highlights the need and opportunity for development of new landscape attributes that
493 characterize the subsurface, echoing the call by Tarasova et al. (2023) and do Nascimento et al., (2025).

494

495 In four of the six regions, soil texture, particularly silt or clay fraction, was identified as a recurring primary driver (Fig. 6b),
496 though their roles differ by context. In the Northeast, silt dominates variable importance; silt is found in glacial till layer and
497 supports high water storage and baseflow (Shanley et al., 2015) while facilitating subsurface stormflow under wet conditions
498 (Detty and McGuire, 2010). In the South, despite silt being identified as a primary driver, clay is the dominant soil texture in
499 many areas (Miller and White, 1998); in the Mississippi embayment, extensive confining units of clay and silt separate aquifers
500 and control the groundwater flow (Renken, 1998; Clark et al., 2011). These two cases suggest that Shapley or permutation-
501 based methods may not fully separate correlated variables due to their treatment of joint variable distributions, and high clay
502 content may be implicitly captured through the absence of silt in regional analyses.

503 **5.2 Informing model selection and evaluation**

504 Our results support hydrological modeling by enabling hydrologists to check whether key processes in a watershed are well-
505 represented by a candidate model prior to application. A wide range of hydrologic models with differing process
506 representations, structures and complexities are available (Knoben et al., 2020). Hydrologists must make choices on whether
507 to include simulations of additional processes such as snowpack or deep groundwater, and the complexity required such as
508 including energy balance at the land surface. Our maps of hydrologic processes provide a pre-screening tool to match
509 hydrological models with appropriate process representations to regions. This approach aims to reduce model structural errors
510 by discouraging use of models ill-suited to the dominant processes (e.g., using a bucket model in overland flow-dominated
511 regions).

512

513 Many previous studies have assessed preferred model structure in individual research watersheds, often using in-depth data
514 analysis to ensure that modeled processes are consistent with observed processes (e.g. Hrachowitz et al., 2014; Kavetski and
515 Fenicia, 2011). This study provides a method to support transparent model justification in applied studies without the resources

516 to conduct model structure investigations, and to upscale model structure decisions to large domains. For example, if selecting
517 models from the MARRMoT toolbox (Knoben et al., 2020), models for regions of dominant overland flow should include
518 saturation excess and/or infiltration excess pathways, and models for regions of complex storage and retention should include
519 multiple parallel groundwater reservoirs. The ability to choose appropriate models for thousands of watersheds is needed for
520 new, flexible model frameworks such as the U.S. Next-Generation National Water Model Framework (Cosgrove et al., 2024;
521 Johnson et al., 2023; Ogden et al., 2021). Our observation-based method complements previous large-domain model-based
522 methods that use analysis of model sensitivities (Markstrom et al., 2016) and performance (Prieto et al., 2021; Spieler et al.,
523 2020) Therefore, where hydrologists seek to evaluate models against process representation, this study offers an opportunity
524 to enhance model benchmarking frameworks by adding process realism as a metric.

525 **5.3 Limitations and future work**

526 The hydrologic process maps produced by this study are limited to the contiguous U.S.. Recent streamflow observation datasets
527 offer the opportunity to extend this method to other regions or globally. Such datasets include the community Caravan dataset
528 (Kratzert et al., 2023), and the international dataset of watersheds with limited human influences, Reference Observatory of
529 Basins for International hydrological climate change detection (ROBIN; Turner et al., 2025). If extending the method globally,
530 caution is advised with scaling, in order to represent different ranges of signature values in different regions. In this study, we
531 plotted signature values as quantiles based on the U.S. distribution, but other countries may have very different signature
532 distributions (McMillan et al., 2022). Therefore, watershed processes that are considered important in a U.S. context, may be
533 considered less important in a global context. Further, some regions of the U.S. are excluded or poorly represented in the
534 dominant process maps presented in this paper, due to a low spatial coverage of USGS stream gages. For example, there are
535 significant gaps in the arid southwest where perennial streamflow is rare (Kiang et al., 2013; Krabbenhoft et al., 2022). In such
536 regions there is a need for alternative process-mapping methods that do not rely on streamflow records.

537
538 Hydrological signatures in this study are long-term averages of the multi-year streamflow dynamics, which may not fully
539 capture temporal variability in watershed processes. Future studies should account for long-term hydroclimatic changes
540 (Hobeichi et al., 2022; Gudmundsson et al., 2025), as well as inter-annual variability (Vogel et al., 1994) and seasonal
541 variations in watershed function (Payn et al., 2012; Gomi et al., 2008). Another complication is that hydrologic signatures are
542 often confounded by multiple processes (McMillan et al., 2020, 2023), whether driven by natural flow dynamics or impaired
543 by human activities. For example, water abstraction by reservoirs reduces downstream flow variability and increases water
544 balance deficits (Salwey et al., 2022; Veldkamp et al., 2016), but changes in vegetation or climate could induce similar effects.
545 Disentangling these impacts remains challenging without testing narrower hypotheses about watershed function, incorporating
546 expert knowledge, or having detailed information about human interventions. In this study, we partially mitigated this issue
547 by using multiple signatures to characterize processes, and by representing human alteration through population density, which
548 showed strong explanatory power for the signatures. Nevertheless, considerable effort is still needed to isolate the combined

549 impacts of multiple processes, as well as the effects of urban development and agricultural practices on flow dynamics
550 (Grantham et al., 2022) for improving the large-scale application of signatures.

551

552 A limitation of this study that would become more apparent at a global scale is the quality of precipitation, streamflow, and
553 attribute data. A previous study noted issues with limited quality and consistency of the global attribute data for soils and
554 geology that reduced their predictive power (Beck et al., 2015). Continental scales necessitate the use of gridded precipitation
555 products, but in areas with low density of observations these products may be insufficient to analyze localized, flashy processes
556 such as infiltration excess flow (McMillan et al., 2023). In small, headwater watersheds, precipitation grid size may be large
557 compared to watershed area, and headwaters are also underrepresented in streamflow observations (Golden et al., 2025).
558 Additionally, errors in watershed boundary delineation would affect signatures that use drainage area to normalize flow, such
559 as runoff ratio (*Total Runoff Ratio*, *Event Runoff Ratio*) and water balance (*Average Storage*). In snowy areas, signature values
560 can be compromised because liquid water inputs to the watershed come from snowmelt rather than directly from precipitation.
561 In our study, we excluded snow-dominated watersheds for signatures related to overland flow, as these require event-scale
562 surface water input that are particularly affected by frozen or snowmelt conditions. Products such as NLDAS3 (Case et al.,
563 2025) or surface water inputs considering rain-on-snow and snowmelt (Hammond, 2024; Hammond and Kampf, 2020) may
564 provide future abilities to estimate overland flow processes in snow areas using estimates of hourly snow accumulation and
565 melt. While our study used potential evapotranspiration (PET) information in only one signature (*Average Storage*),
566 uncertainty in PET is a major issue of global datasets and needs to be addressed (Clerc-Schwarzenbach et al., 2024; Destouni
567 and Zarei, 2024) before this approach can be expanded to a variety of (eco)hydrologic processes.

568

569 A further limitation is the extent to which continental scale maps of dominant processes can be validated. Large-domain
570 signature datasets can be evaluated for data quality, for interpolation quality using cross-validation, and compared with
571 previous datasets. However, it is more difficult to determine how accurately signatures relate to processes over large domains.
572 Research watersheds offer “ground truth” points at which processes are already well understood (Penna, 2024). Previous
573 studies used a handful of U.S. critical zone observatory watersheds for evaluation (McMillan et al., 2022). However, the large
574 number of past and present research watersheds across the globe offer an interesting future opportunity for wider-scale
575 validation of process mapping techniques (McMillan et al., 2025; Sebestyen et al., 2025). Similarly, validation of process
576 drivers remains challenging. While Shapley values and permutation importance provide explanatory power for random forest
577 models, they have some limitations. Both metrics characterize model interactions within a given dataset; therefore, the variety
578 of processes covered in the dataset matters, and data or model uncertainties may propagate into the interpretations (Husic,
579 2025). Shapley values do not capture joint distributional effects among multiple interacting variables (Lundberg and Lee,
580 2017). Developing an explanatory framework that maximizes both model performance and interpretability remains an ongoing
581 research area in hydrology (Robert Maier et al., 2024; Willard et al., 2024).

582 **6 Conclusion**

583 A fundamental question in hydrology is how hydrologic processes are organized over large scales, and how they are controlled
584 by climate and landscape (Blöschl et al., 2019). In this study, we contribute towards answering this question by mapping
585 hydrologic processes and their drivers across the contiguous U.S.. Our approach used hydrologic signatures to describe
586 streamflow dynamics, and connected these dynamics to dominant processes in the associated watersheds using established
587 relationships between signatures and watershed processes. We analyzed 14,146 gauged U.S. watersheds; our map of processes
588 was based on observational data from 10,261 gauged sites and extended using random forest predictions to an additional 3,885
589 watersheds with insufficient record length or completeness. Our method enables knowledge transfer from gauged basins with
590 well-established conceptual models to ungauged or poorly instrumented watersheds.

591
592 Our results comprise maps of hydrologic process importance across the contiguous U.S., including baseflow, overland flow,
593 water storage, seasonal variation and water balance processes. Using interpretable machine learning methods, we create maps
594 of process drivers that explain which climate and landscape attributes are dominant in controlling hydrologic processes in each
595 watershed and each region. We find clear patterns at the continental scale in hydrologic processes, with infiltration excess
596 overland flow dominating the high plains., saturation excess flow prevalent in the valleys of the Tennessee-Missouri region,
597 and varying baseflow contributions across regions. The novelty of this study is in demonstrating that incorporating more
598 detailed landscape attribute elucidates non-climate variables as dominant controls on hydrologic processes, even with a large
599 sample across multiple climate regions. Specifically, the results showed that climate primarily controls hydrologic processes
600 in the western U.S., while soils and geology dominate in the Great Lakes region, topography controls processes in the Southeast,
601 and human influences are most important around large cities across the East.

602
603 Our findings extend and generalize process understanding from research watersheds to large domains, revealing regional
604 heterogeneity within broader physiographic provinces that are often treated as hydrologically uniform. Hydrologic process
605 maps provide essential support for new, large-domain model frameworks that must select model structure across thousands of
606 watersheds. These maps enable hydrologists to select models that adequately represent the dominant processes of a watershed.
607 Identification of dominant processes in each region further enables hydrologists to anticipate streamflow response to
608 environmental change, by identifying which processes are most sensitive to shifts in driving variables. Such analysis has the
609 potential to support scenario testing for future land use or climate, to guide selection of green and grey infrastructure compatible
610 with dominant processes, and to inform risk assessments for regions prone to flash flooding, streamflow depletion, or altered
611 seasonal flow regimes.

612 **Code availability**

613 Code used for analysis is available at <https://doi.org/10.5281/zenodo.20185650> and as a continuously updated version via
614 GitHub at <https://github.com/RY4GIT/signature-prediction> and
615 at https://github.com/RY4GIT/Wetland_GeologicAge_Attributes. Caravan attributes for GAGES-II only watersheds were
616 calculated using <https://github.com/kratzert/Caravan> (Kratzert et al., 2023). Hydrologic signatures are calculated using
617 <https://github.com/RY4GIT/TOSSH>, which modified the original TOSSH toolbox <https://github.com/TOSSHtoolbox/TOSSH>
618 (Gnann et al., 2021b).

619 **Data availability**

620 The process maps in Figures 2 and 3 are available as interactive maps at <https://ry4git.github.io/maps/sig-prediction.html>. The
621 hydrologic signature datasets, derived from observed data and predicted using random forest models, are deposited at
622 <https://doi.org/10.5281/zenodo.20185650>. The Caravan Version 1.5 dataset is available at
623 <https://doi.org/10.5281/zenodo.10968468> (Kratzert et al., 2024), which contains streamflow, meteorological data, watershed
624 boundaries and attributes. GAGES-II attributes are available at
625 <https://www.sciencebase.gov/catalog/item/631405bbd34e36012efa304a> (Falcone, 2011), and time series of meteorological
626 data for GAGES-II locations are available from <https://www.sciencebase.gov/catalog/item/64134069d34eb496d1ce3c6f>
627 (Wieczorek et al., 2023) and <https://www.sciencebase.gov/catalog/item/6494515fd34ef77fcb014eb0> (Hammond, 2024).
628 CAMELSH hourly NLDAS forcings are available at <https://doi.org/10.5281/zenodo.15066778> and
629 <https://doi.org/10.5281/zenodo.15070091> (Tran et al., 2025).

630 **Author contribution**

631 **RA:** conceptualization, data curation, formal analysis, investigation, methodology, software, visualization, writing — original
632 draft preparation, writing — review and editing. **AHo:** conceptualization, data curation, methodology, software, writing —
633 review and editing. **JCH:** data curation, formal analysis, methodology, writing — original draft preparation, writing — review
634 and editing. **AHu:** formal analysis, investigation, methodology, writing — original draft preparation, writing — review and
635 editing. **GC:** investigation, writing — review and editing. **HKM:** funding acquisition, project administration, conceptualization,
636 formal analysis, investigation, methodology, writing — original draft preparation, writing — review and editing, supervision.

637 **Competing interests**

638 At least one of the (co-)authors is a member of the editorial board of Hydrology and Earth System Sciences. The peer-review
639 process was guided by an independent editor, and the authors also have no other competing interests to declare.

640 **Acknowledgement**

641 We thank Sebastian Gnann for the development of the TOSSH toolbox and for the collaborative discussions around my pull
642 requests, Yueling Ma for helpful input on interpretable Machine Learning methods during a conference, and Andy Wood for
643 valuable feedback about anthropogenic impacts on streamflow patterns and signatures. The bivariate map was inspired by a
644 blogpost written by Muhammad Mohsin Raza on their website DataWim. We thank Roy Sando and Scott Hamshaw for helpful
645 feedback on the earlier version of the manuscript. We appreciate the computing support provided by the IT team at the
646 Department of Geography, San Diego State University, and the General Research IT (GRIT) team at the University of
647 California, Santa Barbara. Any use of trade, firm, or product names is for descriptive purposes only and does not imply
648 endorsement by the U.S. government.

649 **Financial Support**

650 Araki, Holt, McMillan were supported by the NSF Hydrologic Sciences Program, Division of Earth Sciences, Award Number
651 2124923. Araki acknowledges support from the Shida Scholarship Program. Coxon was supported by a UKRI Future Leaders
652 Fellowship [MR/V022857/1].

653

655 **Table 1:** Hydrologic signatures used for building process hypotheses. The signature descriptions are adapted from
 656 (McMillan et al., 2022).

Hydrologic processes and signature hypothesis	Relationship between the signature values and process strength	Signature (variable name in dataset)	Unit	Description
Baseflow We hypothesize that a larger baseflow magnitude (i.e., higher <i>Baseflow Index</i>) and a slower recession rate (i.e., lower <i>Baseflow Recession K</i>) indicate a stronger baseflow process.	Positive	<i>Baseflow Index (BFI)</i>	-	Baseflow index (BFI) represents baseflow proportion and residence time (Bulygina et al., 2009; Yilmaz et al., 2008). Calculated as mean baseflow divided by mean streamflow. Hydrograph separation is implemented to obtain baseflow fraction using the UKIH smoothed minima method (UKIH, 1980).
	Negative	<i>Baseflow Recession K (BaseflowRecessionK)</i>	1/d	Represents groundwater influence and longer subsurface flow paths (Safeeq et al., 2013). Calculated as an exponential recession constant K fitted to the master recession curve derived from adaptive matching strip method.
High storage capacity We hypothesize that larger storage (i.e., higher <i>Average Storage</i>) and more nonlinear recession patterns (i.e., higher <i>Recession Parameter b</i>) indicate a greater storage capacity and the involvement of multiple storages.	Positive	<i>Average Storage (AverageStorage)</i>	mm	Represents average magnitude of watershed storage (Peters and Aulenbach, 2011). Derived from average baseflow and storage-discharge relationship. Uses a simple water balance model to calculate changes in storage, then finds the relationship between storage and discharge, and then estimates average storage from average baseflow.
	Positive	<i>Recession Parameter b (RecessionParameters_b)</i>	-	The nonlinearity indicates the contributions of multiple storages (Clark et al., 2009; Tallaksen, 1995). Recession analysis parameters approximate storage-discharge relationship. Fits a line to the $dQ/dt-Q$ relationship in log-log space for each individual recession and returns the median slope. b is a shape parameter representing the degree of nonlinearity.
Water balance losses We hypothesize that a smaller runoff ratio (Q:P ratio) at both interannual and event scales (i.e., lower <i>Total Runoff Ratio</i> and <i>Event Runoff Ratio</i>) indicates greater water balance losses due to evapotranspiration, deep drainage to groundwater, or some other processes.	Negative	<i>Total Runoff Ratio (TotalRR)</i>	-	Total runoff ratio (RR) infer evapotranspiration or other flow bypassing gauge (Safeeq and Hunsaker, 2016). Calculated as mean streamflow divided by mean precipitation.
	Negative	<i>Event Runoff Ratio (EventRR)</i>	-	Event runoff ratio (RR) infer rapid vertical drainage of water to groundwater (Noguchi et al., 1997). Calculated as an average of runoff ratios (streamflow divided by precipitation) from all identified storm events.

<p>Seasonal variability</p> <p>We hypothesize that greater flow variability, both in general patterns (i.e., higher <i>Variability Index</i>) and in seasonal patterns (i.e., higher <i>Recession Seasonality</i>), indicates a stronger influence of seasonal evapotranspiration patterns on water storage.</p>	Positive	<i>Recession Seasonality (Recession_a_Seasonality)</i>	-	Seasonal variation in the recession “a” parameter reflects the impact of evapotranspiration on water storage (Shaw and Riha, 2012). Calculated as the difference between the maximum and minimum monthly median values of the y-intercept (“a” parameter) in the $dQ/dt-Q$ relationship in log-log space, assuming a slope of 2.
	Positive	<i>Variability Index (VariabilityIndex)</i>	-	High variability index shows lower water storage (Estrany et al., 2010). Calculated as the standard deviation of log-transformed discharge values determined at 10% intervals from 10% to 90% of the cumulative frequency distribution (flow duration curve).
<p>Overland flow</p> <p>We hypothesized that a strong threshold relationship between quickflow and precipitation characteristics (i.e., high significance and higher threshold values) suggests a more dominant overland flow process.</p>	Negative (Values outside the range $0 \leq P\text{-value} \leq 0.05$ are deemed insignificant and clipped out. Within the range, the smaller P-value is, the more significant the threshold is)	Average of <i>IE Threshold Significance (IE_thresh_signif)</i> and <i>SE Threshold Significance (SE_thresh_signif)</i>	-	Significant values (<0.05) imply infiltration excess (IE) or saturation excess (SE) occurs (Ali et al., 2013; McGrath et al., 2007). <i>p</i> -value was calculated for the significance of a non-zero change in slope above and below a threshold in a relationship of event quickflow volume versus event maximum precipitation intensity (for IE) or event total precipitation volume (for SE).
	Positive	Average of <i>IE Threshold (IE_thresh)</i> and <i>SE Threshold (SE_thresh)</i>	mm	Indicates rainfall intensity or event precipitation depth required to generate infiltration excess or saturation excess, respectively (Ali et al., 2013; McGrath et al., 2007). Value of the threshold identified in the <i>IE/SE_thresh_signif</i> signature. The “broken-stick” model was fit to the relationship between quickflow vs. precipitation characteristics.
<p>Overland flow type</p> <p>We hypothesized that the relative strength in infiltration vs. saturation of excess overland flow (i.e., differences in <i>IE Correlation</i> and <i>SE Correlation</i>) indicate the prevalence of either overland flow mechanisms.</p> <p>Exclude watersheds where event runoff coefficient has negative relationships with storm characteristics (i.e., <i>SE Correlation</i> < 0 and <i>IE Correlation</i> < 0).</p>	Positive relationship with infiltration excess overland flow	<i>IE Correlation (RC_Pint)</i>	-	Indicates stormflow processes sensitive to rainfall intensity, for example, infiltration excess (Hortonian) overland flow (Wu et al., 2021). Calculated as the Spearman correlation coefficients between event runoff coefficient and event maximum rainfall intensity. As per (Wu et al., 2021), event maximum rainfall intensity is calculated as the multiplication of daily rainfall (mm/day) from original climate forcings (i.e., ERA5 for Caravan, gridMET for GAGES-II) multiplied by the fraction of maximum rainfall intensity from CAMELSH hourly NLDAS forcings.
	Positive relationship with saturation excess overland flow	<i>SE Correlation (RC_Pvol)</i>	-	Indicates stormflow processes sensitive to rainfall volume, for example, saturation excess overland flow, subsurface stormflow, and groundwater flow (Wu et al., 2021). Calculated as the Spearman correlation coefficients between event runoff coefficient and rainfall volume.

657

658 **Table 2:** Landscape attributes used in training the random forest model. Descriptions are adapted from (Falcone, 2011;
659 Falcone et al., 2010; Holt and McMillan, 2025; Kratzert et al., 2023; Linke et al., 2019). For predictions, when certain
660 attributes are unavailable, equivalent attributes are substituted (e.g., Caravan equivalents are used when predicting signatures
661 for watershed samples available only in Caravan). The combinations are detailed in Table S1. An asterisk (*) in the unit
662 column indicates that the landscape attribute unit from GAGES-II was converted to the Caravan equivalent (Fig. S11 shows
663 the comparison).

664

Category	Attribute Name (variable name in attribute dataset)	Description	Unit	Original Source	Dataset Source	Caravan Equivalent
Physiography	Elevation (ELEV_MEAN_M_BASIN)	Mean watershed elevation	meters	USGS 100m National Elevation Dataset (Gesch et al., 2018)	GAGES-II	ele_mt_sav
Physiography	Watershed area (DRAIN_SQKM)	Watershed drainage area	km ²	Multiple sources, while the majority derived from NHDPlus (U.S. Environmental Protection Agency, 2008) (see original USGS, 2011 report on GAGES-II)	GAGES-II	area
Physiography	Slope (SLOPE_DEG)	Mean watershed slope, percent	%	USGS 100m resolution National Elevation Dataset (Gesch et al., 2018)	GAGES-II	slp_dg_sav
Land Cover	Forest (FORESTNLCD06)	Forest extent	% area	NLCD06 for most regions; NLCD01 for Alaska, Hawaii, and Puerto Rico (Yang et al., 2018)	GAGES-II	for_pc_sse
Land Cover	Cropland (CROPSNLCD06)	Cultivated Crops extent	% area		GAGES-II	crp_pc_sse
Land Cover	Pasture (PASTURENLCD06)	Pasture/Hay extent	% area		GAGES-II	pst_pc_sse
Land Cover	Irrigated agriculture (PCT_IRRIG_AG)	Irrigated agriculture extent	% area	Based on 250m MODIS datasets, USGS M1RAD-US (Shrestha et al., 2019)	GAGES-II	ire_pc_sse
Land Cover	Protected area (PADCAT1_AND_2)	Percent of watershed designated as Protected Area Category 1 and 2	% area *	Protected Areas Database (United States Geological Survey, 2024)	GAGES-II	pac_pc_sse

Land Cover	Isolated wetland (isowet_arefrac)	Isolated wetland area fraction (Holt, 2024)	-	National Wetlands Inventory (Lane and D'Amico, 2016)	Holt and McMillan, 2025	N/A
Soils & Geology	Clay fraction (CLAYAVE)	Average clay content	%	STATSGO (United States Department of Agriculture et al., 2008)	GAGES-II	cly_pc_sav
Soils & Geology	Silt fraction (SILTAVE)	Average silt content	%		GAGES-II	slt_pc_sav
Soils & Geology	Soil organic carbon (soc_th_sav)	Organic carbon content in soil	tonnes/hectare		Caravan/HydroAtlas	N/A
Soils & Geology	Karst (kar_pc_sse)	Karst area extent	% area	Rock Outcrops v3.0 (Williams and Ford, 2006)	Caravan/HydroAtlas	N/A
Soils & Geology	Geologic age (geol_weighted_ave_age_ma)	Area-weighted average of geologic age	ma	The USGS State Geologic Map Compilation (Horton et al., 2017)	Holt and McMillan, 2025	N/A
Anthropogenic	Population density (PDEN_2000_BLOCK)	Population density in the watershed	persons/km ²	2000 Census block data regridded to 100m	GAGES-II	ppd_pk_sav
Climate	Precipitation (P_mm_day)	Mean annual precipitation (1971-2000). The unit was converted from the original variable "PPTAVG_BASIN" in cm/year to mm/day.	mm/day *	800m PRISM data	GAGES-II	p_mean
Climate	PET (PET_mm_day)	Mean annual potential evapotranspiration rate estimated from mean monthly air temperature and latitude using Hamon (1961) equation. The unit was converted from the original variable "PET" in mm/year to mm/day.	mm/day *	Monthly air temperature from 30-year (1961-1990) PRISM	GAGES-II	pet_mean_FAO_PM

Climate	Aridity (ARIDITY_GAGES2)	Aridity index, ratio of mean PET and mean precipitation	-	Calculated from PPTAVG_BASIN and PET in GAGES-II attributes	GAGES-II	aridity_FAO_PM
Climate	Snow fraction (SNOW_PCT_PRECIP)	Mean snow percent of total precipitation estimate (1901-2000)	- *	McCabe and Wolock (submitted, 2008), 1km grid	GAGES-II	frac_snow
Climate	Seasonality (seasonality_FAO_PM)	Moisture index seasonality in range [0, 2] (Knoben et al., 2018), where 0 indicates no change in the water or energy budget throughout the year, and 2 indicates a transition from fully arid to fully humid conditions. The moisture index is calculated as the normalized aridity index at the monthly scale.	-	ERA-5 (Muñoz Sabater, 2019); The FAO Penman–Monteith equation (Allen et al., 1998; Shalev and Kratzert, 2024) is used to calculate Potential Evapotranspiration (PET)	Caravan/ERA-5	N/A
Climate	High precipitation frequency (high_prec_freq)	Frequency of high precipitation days, where precipitation ≥ 5 times mean daily precipitation	-	ERA-5 (Muñoz Sabater, 2019)	Caravan/ERA-5	N/A
Climate	Low precipitation frequency (low_prec_freq)	Frequency of low precipitation days, where precipitation < 1 mm/day	-	ERA-5 (Muñoz Sabater, 2019)	Caravan/ERA-5	N/A
Climate	Low precipitation duration (low_prec_dur)	Average duration of low precipitation events (number of consecutive	day	ERA-5 (Muñoz Sabater, 2019)	Caravan/ERA-5	N/A

		days where precipitation <1 mm/day)				
--	--	-------------------------------------	--	--	--	--

665 **References**

666 Abban, B., Papanicolaou, A. N. (thanos), Cowles, M. K., and Wilson, C. G.: Examining Seasonal Trends in Sediment Source
667 Contributions in an Intensely Cultivated Midwestern Sub-Watershed Using Bayesian Unmixing, in: World Environmental and
668 Water Resources Congress 2014, World Environmental and Water Resources Congress 2014, Portland, Oregon, 1453–1463,
669 <https://doi.org/10.1061/9780784413548.146>, 2014.

670 Addor, N., Newman, A. J., Mizukami, N., and Clark, M. P.: The CAMELS data set: catchment attributes and meteorology for
671 large-sample studies, *Hydrol. Earth Syst. Sci.*, 21, 5293–5313, <https://doi.org/10.5194/hess-21-5293-2017>, 2017.

672 Addor, N., Nearing, G., Prieto, C., Newman, A. J., Le Vine, N., and Clark, M. P.: A ranking of hydrological signatures based
673 on their predictability in space, *Water Resour. Res.*, 54, 8792–8812, <https://doi.org/10.1029/2018WR022606>, 2018.

674 Ali, G., Tetzlaff, D., Soulsby, C., McDonnell, J. J., and Capell, R.: A comparison of similarity indices for catchment
675 classification using a cross-regional dataset, *Adv. Water Resour.*, 40, 11–22, <https://doi.org/10.1016/j.advwatres.2012.01.008>,
676 2012.

677 Ali, G., Oswald, C. J., Spence, C., Cammeraat, E. L. H., McGuire, K. J., Meixner, T., and Reaney, S. M.: Towards a unified
678 threshold-based hydrological theory: necessary components and recurring challenges: INVITED COMMENTARY, *Hydrol.*
679 *Process.*, 27, 313–318, <https://doi.org/10.1002/hyp.9560>, 2013.

680 Allen, R. G., Pereira, L. S., Raes, D., and Smith, M.: Crop Evapotranspiration – Guidelines for Computing Crop Water
681 Requirements, in: FAO Irrigation and drainage paper 56, Food and Agriculture Organization of the United Nations, Rome,
682 Italy, 1998.

683 Almagro, A., Meira Neto, A. A., Vergopolan, N., Roy, T., Troch, P. A., and Oliveira, P. T. S.: The Drivers of Hydrologic
684 Behavior in Brazil: Insights From a Catchment Classification, *Water Resources Research*, 60,
685 <https://doi.org/10.1029/2024WR037212>, 2024.

686 Angermann, L., Jackisch, C., Allroggen, N., Sprenger, M., Zehe, E., Tronicke, J., Weiler, M., and Blume, T.: Form and function
687 in hillslope hydrology: characterization of subsurface flow based on response observations, *Hydrol. Earth Syst. Sci.*, 21, 3727–
688 3748, <https://doi.org/10.5194/hess-21-3727-2017>, 2017.

689 Araki, R., Branger, F., Wiekenkamp, I., and McMillan, H. K.: A signature-based approach to quantify soil moisture dynamics
690 under contrasting land-uses, *Hydrol. Process.*, 36, e14553, <https://doi.org/10.1002/hyp.14553>, 2022.

691 Ariano, S. and Ali, G.: From river flow regime diversity to proxies for hydrologic homogeneity a Canada-wide case study, *Sci.*
692 *Rep.*, 15, 16743, <https://doi.org/10.1038/s41598-025-00244-7>, 2025.

693 Arsenault, R., Brissette, F., Martel, J.-L., Troin, M., Lévesque, G., Davidson-Chaput, J., Gonzalez, M. C., Ameli, A., and
694 Poulin, A.: A comprehensive, multisource database for hydrometeorological modeling of 14,425 North American watersheds,
695 *Sci Data*, 7, 243, <https://doi.org/10.1038/s41597-020-00583-2>, 2020.

696 Barnhart, T. B., Molotch, N. P., Livneh, B., Harpold, A. A., Knowles, J. F., and Schneider, D.: Snowmelt baseflow
697 contributions: A comparison of methods using nested catchments in the Colorado River basin, *Water Resources Research*, 52,
698 4524–4548, 2016.

699 Barnhart, T. B., Farmer, W. H., Hammond, J. C., Sexstone, G. A., Curran, J. H., Koch, J. C., and Driscoll, J. M.: Evaluating
700 hydrologic region assignment techniques for ungaged basins in Alaska, USA, *River Res. Appl.*, 38, 1569–1584,
701 <https://doi.org/10.1002/rra.4028>, 2022.

702 Beck, H., Dijk, A., Miralles, D., Jeu, R. A. M., (Sampurno) Bruijnzeel, L., McVicar, T., and Schellekens, J.: Global patterns
703 in base flow index and recession based on streamflow observations from 3394 catchments, *Water Resources Research*, 49,
704 7843–7863, <https://doi.org/10.1002/2013WR013918>, 2013.

705 Beck, H. E., De Roo, A., and van Dijk, A. I.: Global maps of streamflow characteristics based on observations from several
706 thousand catchments, *J. Hydrometeorol.*, 16, 1478–1501, 2015.

707 Bergström, S.: *The HBV Model: Its Structure and Applications*, Swedish Meteorological and Hydrological Institute (SMHI),
708 Hydrology, Norrköping, 35 pp., 1992.

709 Berghuijs, W. R., Sivapalan, M., Woods, R. A., and Savenije, H. H. G.: Patterns of similarity of seasonal water balances: A
710 window into streamflow variability over a range of time scales, *Water Resour. Res.*, 50, 5638–5661,
711 <https://doi.org/10.1002/2014WR015692>, 2014.

712 Blöschl, G.: Hydrologic synthesis: Across processes, places, and scales, *Water Resour. Res.*, 42,
713 <https://doi.org/10.1029/2005wr004319>, 2006.

714 Blöschl, G., Bierkens, M. F. P., Chambel, A., Cudennec, C., Destouni, G., Fiori, A., Kirchner, J. W., McDonnell, J. J., Savenije,
715 H. H. G., Sivapalan, M., Stumpp, C., Toth, E., Volpi, E., Carr, G., Lupton, C., Salinas, J., Széles, B., Viglione, A., Aksoy, H.,
716 Allen, S. T., Amin, A., Andréassian, V., Arheimer, B., Aryal, S. K., Baker, V., Bardsley, E., Barendrecht, M. H., Bartosova,
717 A., Batelaan, O., Berghuijs, W. R., Beven, K., Blume, T., Bogaard, T., Borges de Amorim, P., Böttcher, M. E., Boulet, G.,
718 Breinl, K., Brilly, M., Brocca, L., Buytaert, W., Castellarin, A., Castelletti, A., Chen, X., Chen, Y., Chen, Y., Chiffard, P.,
719 Claps, P., Clark, M. P., Collins, A. L., Croke, B., Dathe, A., David, P. C., de Barros, F. P. J., de Rooij, G., Di Baldassarre, G.,
720 Driscoll, J. M., Duethmann, D., Dwivedi, R., Eris, E., Farmer, W. H., Feiccabrino, J., Ferguson, G., Ferrari, E., Ferraris, S.,
721 Fersch, B., Finger, D., Foglia, L., Fowler, K., Gartsman, B., Gascoïn, S., Gaume, E., Gelfan, A., Geris, J., Gharari, S., Gleeson,
722 T., Glendell, M., Gonzalez Bevacqua, A., González-Dugo, M. P., Grimaldi, S., Gupta, A. B., Guse, B., Han, D., Hannah, D.,
723 Harpold, A., Haun, S., Heal, K., Helfricht, K., Herrnegger, M., Hipsey, M., Hlaváčiková, H., Hohmann, C., Holko, L.,
724 Hopkinson, C., Hrachowitz, M., Illangasekare, T. H., Inam, A., Innocente, C., Istanbuluoglu, E., Jarihani, B., et al.: Twenty-
725 three unsolved problems in hydrology (UPH) – a community perspective, *Hydrol. Sci. J.*, 64, 1141–1158,
726 <https://doi.org/10.1080/02626667.2019.1620507>, 2019.

727 Bolotin, L. A. and McMillan, H.: A hydrologic signature approach to analysing wildfire impacts on overland flow, *Hydrol.*
728 *Process.*, 38, <https://doi.org/10.1002/hyp.15215>, 2024.

729 Bracken, L. J., Wainwright, J., Ali, G. A., Tetzlaff, D., Smith, M. W., Reaney, S. M., and Roy, A. G.: Concepts of hydrological
730 connectivity: Research approaches, pathways and future agendas, *Earth-Sci. Rev.*, 119, 17–34,
731 <https://doi.org/10.1016/j.earscirev.2013.02.001>, 2013.

732 Brooks, P. D., Chorover, J., Fan, Y., Godsey, S. E., Maxwell, R. M., McNamara, J. P., and Tague, C.: Hydrological partitioning
733 in the critical zone: Recent advances and opportunities for developing transferable understanding of water cycle dynamics:
734 CRITICAL ZONE HYDROLOGY, *Water Resour. Res.*, 51, 6973–6987, <https://doi.org/10.1002/2015wr017039>, 2015.

735 Brunner, M. I., Melsen, L. A., Newman, A. J., Wood, A. W., and Clark, M. P.: Future streamflow regime changes in the United
736 States: assessment using functional classification, *Hydrol. Earth Syst. Sci.*, 24, 3951–3966, [https://doi.org/10.5194/hess-24-](https://doi.org/10.5194/hess-24-3951-2020)
737 [3951-2020](https://doi.org/10.5194/hess-24-3951-2020), 2020.

738 Buchanan, B., Auerbach, D. A., Knighton, J., Evensen, D., Fuka, D. R., Easton, Z., Wieczorek, M., Archibald, J. A.,
739 McWilliams, B., and Walter, T.: Estimating dominant runoff modes across the conterminous United States, *Hydrol. Process.*,
740 32, 3881–3890, <https://doi.org/10.1002/hyp.13296>, 2018.

741 Bulygina, N., McIntyre, N., and Wheeler, H.: Conditioning rainfall-runoff model parameters for ungauged catchments and
742 land management impacts analysis, *Hydrol. Earth Syst. Sci.*, 13, 893–904, <https://doi.org/10.5194/hess-13-893-2009>, 2009.

743 Case, J. L., Mocko, D. M., Hain, C. R., Maina, F. Z., Whitney, K. M., Kumar, S. V., Wade, R. A., Locke, K. A., and White,
744 K. D.: NLDAS-3: Next-Generation Land Data Assimilation System to Support North American Water-Informed Decisions,
745 in: 2025 National Soil Moisture Workshop, 2025.

746 Clark, M., Rupp, D., Woods, R., Meerveld, H., Peters, N., and Freer, J.: Consistency between hydrological models and field
747 observations: linking processes at the hillslope scale to hydrological responses at the watershed scale, *Hydrological Processes*,
748 23, 311–319, <https://doi.org/10.1002/HYP.7154>, 2009.

749 Clark, M., Nijssen, B., Lundquist, J., Kavetski, D., Rupp, D., Woods, R., Freer, J., Gutmann, E., Wood, A., Brekke, L., Arnold,
750 J., Gochis, D., and Rasmussen, R.: A unified approach for process-based hydrologic modeling: 1. Modeling concept, *Water*
751 *Resources Research*, 51, 2498–2514, <https://doi.org/10.1002/2015WR017198>, 2015.

752 Clerc-Schwarzenbach, F., Selli, G., Neri, M., Toth, E., van Meerveld, I., and Seibert, J.: Large-sample hydrology – a few
753 camels or a whole caravan?, *Hydrol. Earth Syst. Sci.*, 28, 4219–4237, <https://doi.org/10.5194/hess-28-4219-2024>, 2024.

754 Clark, B. R., Hart, R. M., and Gurdak, J.J.: Groundwater Availability of the Mississippi Embayment, U.S. Geological Survey,
755 Reston, Professional Paper 1785, 62p.

756 Cosgrove, B., Gochis, D., Flowers, T., Dugger, A., Ogden, F., Graziano, T., Clark, E., Cabell, R., Casiday, N., Cui, Z., Eicher,
757 K., Fall, G., Feng, X., Fitzgerald, K., Frazier, N., George, C., Gibbs, R., Hernandez, L., Johnson, D., Jones, R., Karsten, L.,
758 Kefelegn, H., Kitzmiller, D., Lee, H., Liu, Y., Mashriqui, H., Mattern, D., McCluskey, A., McCreight, J. L., McDaniel, R.,
759 Midekisa, A., Newman, A., Pan, L., Pham, C., RafieciNasab, A., Rasmussen, R., Read, L., Rezaeianzadeh, M., Salas, F., Sang,
760 D., Sampson, K., Schneider, T., Shi, Q., Sood, G., Wood, A., Wu, W., Yates, D., Yu, W., and Zhang, Y.: NOAA’s National

761 Water Model: Advancing operational hydrology through continental-scale modeling, *J. Am. Water Resour. Assoc.*, 60, 247–
762 272, <https://doi.org/10.1111/1752-1688.13184>, 2024.

763 Davis, C. A., Ward, A. S., Burgin, A. J., Loecke, T. D., Riveros-Iregui, D. A., Schnoebelen, D. J., Just, C. L., Thomas, S. A.,
764 Weber, L. J., and St. Clair, M. A.: Antecedent Moisture Controls on Stream Nitrate Flux in an Agricultural Watershed, *Journal*
765 *of Environmental Quality*, 43, 1494–1503, <https://doi.org/10.2134/jeq2013.11.0438>, 2014.

766 DeCicco, L. A., Hirsch, R. M., Lorenz, D., Watkins, D., and Michael Johnson, J.: dataRetrieval, U.S. Geological Survey,
767 <https://doi.org/10.5066/P9X4L3GE>, 2018.

768 Destouni, G. and Zarei, M.: Water and climate interplay on land in comparative datasets: Revealing unrealistic major drying
769 bias of climate reanalysis over Africa and the world, *AGUFM*, 2024, H54B–05, 2024.

770 Dettinger, M. D. and Diaz, H. F.: Global characteristics of stream flow seasonality and variability, *J. Hydrometeorol.*, 1, 289–
771 310, [https://doi.org/10.1175/1525-7541\(2000\)001<0289:gcossfs>2.0.co;2](https://doi.org/10.1175/1525-7541(2000)001<0289:gcossfs>2.0.co;2), 2000.

772 Detty, J. M. and McGuire, K. J.: Threshold changes in storm runoff generation at a till-mantled headwater catchment, *Water*
773 *Resour. Res.*, 46, <https://doi.org/10.1029/2009wr008102>, 2010.

774 Dhungel, S., Tarboton, D. G., Jin, J., and Hawkins, C. P.: Potential effects of climate change on ecologically relevant
775 streamflow regimes: Climate change and streamflow regimes, *River Res. Appl.*, 32, 1827–1840,
776 <https://doi.org/10.1002/rra.3029>, 2016.

777 Dunne, T.: Field studies of hillslope flow processes, in: *Hillslope hydrology*, vol. 9, edited by: Kirkby, M. J., John Wiley &
778 Sons, Inc., 227–293, <https://doi.org/10.18172/cig.1099>, 1978.

779 do Nascimento, T. V., Rudlang, J., Gnann, S., Seibert, J., Hrachowitz, M., & Fenicia, F.: How do geological map details
780 influence the identification of geology-streamflow relationships in large-sample hydrology studies? *Hydrol. Earth Syst. Sci.*,
781 29(24), 7173-7200. <https://doi.org/10.5194/hess-29-7173-2025>, 2025.

782 Eng, K. and Wolock, D. M.: Evaluation of machine learning approaches for predicting streamflow metrics across the
783 conterminous United States, 2022–5058, 2022.

784 Estrany, J., Garcia, C., and Batalla, R. J.: Hydrological response of a small mediterranean agricultural catchment, *J. Hydrol.*
785 (Amst.), 380, 180–190, <https://doi.org/10.1016/j.jhydrol.2009.10.035>, 2010.

786 Falcone, J.: GAGES-II: Geospatial Attributes of Gages for Evaluating Streamflow, <https://doi.org/10.5066/P96CPHOT>, 2011.

787 Falcone, J. A., Carlisle, D. M., Wolock, D. M., and Meador, M. R.: GAGES: A stream gage database for evaluating natural
788 and altered flow conditions in the conterminous United States, *Ecology*, 91, 621–621, <https://doi.org/10.1890/09-0889.1>, 2010.

789 Fang, K. and Shen, C.: Full-flow-regime storage-streamflow correlation patterns provide insights into hydrologic functioning
790 over the continental US, *Water Resour. Res.*, 53, 8064–8083, <https://doi.org/10.1002/2016wr020283>, 2017.

791 Fan, Y., Clark, M., Lawrence, D. M., Swenson, S., Band, L. E., Brantley, S. L., Brooks, P. D., Dietrich, W. E., Flores, A.,
792 Grant, G., Kirchner, J. W., Mackay, D. S., McDonnell, J. J., Milly, P. C. D., Sullivan, P. L., Tague, C., Ajami, H., Chaney, N.,
793 Hartmann, A., Hazenberg, P., McNamara, J., Pelletier, J., Perket, J., Rouholahnejad-Freund, E., Wagener, T., Zeng, X.,
794 Beighley, E., Buzan, J., Huang, M., Livneh, B., Mohanty, B. P., Nijssen, B., Safeeq, M., Shen, C., Verseveld, W., Volk, J.,

795 and Yamazaki, D.: Hillslope hydrology in global change research and Earth system modeling, *Water Resour. Res.*, 55, 1737–
796 1772, <https://doi.org/10.1029/2018wr023903>, 2019.

797 Fenicia, F. and McDonnell, J. J.: Modeling streamflow variability regional scale:(1) perceptual model development through
798 signature analysis, *Journal Hydrology*, 2022.

799 Frame, J. M., Araki, R., Bhuiyan, S. A., Bindas, T., Rapp, J., Bolotin, L., Deardorff, E., Liu, Q., Haces-Garcia, F., Liao, M.,
800 Frazier, N., and Ogden, F. L.: Machine learning for a heterogeneous water modeling framework, *J. Am. Water Resour. Assoc.*,
801 61, <https://doi.org/10.1111/1752-1688.70000>, 2025.

802 Gesch, D. B., Evans, G. A., Oimoen, M. J., and Arundel, S.: The National Elevation Dataset: USGS Earth Resources
803 Observation and Science Center, 2018.

804 Gnann, S., Baldwin, J. W., Cuthbert, M. O., Gleeson, T., Schwanghart, W., and Wagener, T.: The influence of topography on
805 the global terrestrial water cycle, *Rev. Geophys.*, 63, e2023RG000810, <https://doi.org/10.1029/2023rg000810>, 2025.

806 Gnann, S. J., Howden, N. J. K., and Woods, R. A.: Hydrological signatures describing the translation of climate seasonality
807 into streamflow seasonality, *Hydrol. Earth Syst. Sci. Discuss.*, 24, 561–580, <https://doi.org/10.5194/hess-24-561-2020>, 2020.

808 Gnann, S. J., McMillan, H. K., Woods, R. A., and Howden, N. J. K.: Including Regional Knowledge Improves Baseflow
809 Signature Predictions in Large Sample Hydrology, *Water Resour. Res.*, 57, e2020WR028354,
810 <https://doi.org/10.1029/2020WR028354>, 2021a.

811 Gnann, S. J., Coxon, G., Woods, R. A., Howden, N. J. K., and McMillan, H. K.: TOSSH: A Toolbox for Streamflow Signatures
812 in Hydrology, *Environmental Modelling & Software*, 138, 104983, <https://doi.org/10.1016/j.envsoft.2021.104983>, 2021b.

813 Golden, H. E., Christensen, J. R., McMillan, H. K., Kelleher, C. A., Lane, C. R., Husic, A., Li, L., Ward, A. S., Hammond, J.,
814 Seybold, E. C., Jaeger, K. L., Zimmer, M., Sando, R., Jones, C. N., Segura, C., Mahoney, D. T., Price, A. N., and Cheng, F.:
815 Advancing the science of headwater streamflow for global water protection, *Nat Water*, 1–11, <https://doi.org/10.1038/s44221-024-00351-1>, 2025.

817 Gomi, T., Sidle, R. C., Ueno, M., Miyata, S., & Kosugi, K. (2008). Characteristics of overland flow generation on steep
818 forested hillslopes of central Japan. *Journal of Hydrology*, 361(3-4), 275-290.
819 <https://doi.org/10.1016/j.jhydrol.2008.07.045>

820 Goodrich, D. C., Lane, L. J., Shillito, R. M., Miller, S. N., Syed, K. H., and
821 Woolhiser, D. A.: Linearity of basin response as a function of scale in a semiarid watershed, *Water Resour. Res.*, 33, 2951–
2965, <https://doi.org/10.1029/97wr01422>, 1997.

822 Grantham, T. E., Carlisle, D. M., Howard, J., Lane, B., Lusardi, R., Obester, A., Sandoval-Solis, S., Stanford, B., Stein, E. D.,
823 Taniguchi-Quan, K. T., Yarnell, S. M., and Zimmerman, J. K. H.: Modeling functional flows in California’s rivers, *Front.*
824 *Environ. Sci.*, 10, <https://doi.org/10.3389/fenvs.2022.787473>, 2022.

825 Gudmundsson, L., Brunner, M. I., Döll, P., Fluet-Chouinard, E., Frolova, N., Gosling, S. N., Hirabayashi, Y., Kireeva, M. B.,
826 Liu, X., Müller Schmied, H., Magritskiy, D., Slater, L. J., Stein, L., Trambly, Y., Wang, K., Wasko, C., Yamazaki, D., and
827 Zhou, X.: Past and future change in global river flows, *Nat. Rev. Earth Environ.*, [https://doi.org/10.1038/s43017-025-00745-](https://doi.org/10.1038/s43017-025-00745-z)
828 z, 2025.

829 Haines, A., Finlayson, B., and McMahon, T.: A global classification of river regimes, *Applied Geography*, 8, 255–272,
830 [https://doi.org/10.1016/0143-6228\(88\)90035-5](https://doi.org/10.1016/0143-6228(88)90035-5), 1988.

831 Hammond, J. C.: Daily time series of surface water input from rainfall, rain on snow, and snowmelt for the Conterminous
832 United States from 1990 to 2023, as well as annual series of input seasonality, precipitation seasonality, and average rainfall,
833 rain on snow, and snowmelt rates, <https://doi.org/10.5066/P9JWJPNC>, 2024.

834 Hammond, J. C. and Kampf, S. K.: Subannual streamflow responses to rainfall and snowmelt inputs in snow-dominated
835 watersheds of the western United States, *Water Resour. Res.*, 56, <https://doi.org/10.1029/2019wr026132>, 2020.

836 Hammond, J. C., Zimmer, M., Shanafield, M., Kaiser, K., Godsey, S. E., Mims, M. C., Zipper, S. C., Burrows, R. M., Kampf,
837 S. K., Dodds, W., Jones, C. N., Krabbenhoft, C. A., Boersma, K. S., Detry, T., Olden, J. D., Allen, G. H., Price, A. N., Costigan,
838 K., Hale, R., Ward, A. S., and Allen, D. C.: Spatial patterns and drivers of nonperennial flow regimes in the contiguous United
839 States, *Geophys. Res. Lett.*, 48, <https://doi.org/10.1029/2020gl090794>, 2021.

840 Hammond, J. C., Sexstone, G. A., Putman, A. L., Barnhart, T. B., Rey, D. M., Driscoll, J. M., Liston, G. E., Rasmussen, K. L.,
841 McGrath, D., Fassnacht, S. R., and Kampf, S. K.: High resolution SnowModel simulations reveal future elevation-dependent
842 snow loss and earlier, flashier surface water input for the upper Colorado river basin, *Earths Future*, 11,
843 <https://doi.org/10.1029/2022ef003092>, 2023.

844 Hay, L. E., LaFontaine, J. H., Van Beusekom, A. E., Norton, P. A., Farmer, W. H., Regan, R. S., Markstrom, S. L., and
845 Dickinson, J. E.: Parameter estimation at the conterminous United States scale and streamflow routing enhancements for the
846 National Hydrologic Model infrastructure application of the Precipitation-Runoff Modeling System (NHM-PRMS),
847 <https://doi.org/10.3133/tm6b10>, 2023.

848 Hobeichi, S., Abramowitz, G., Ukkola, A. M., De Kauwe, M., Pitman, A., Evans, J. P., and Beck, H.: Reconciling historical
849 changes in the hydrological cycle over land, *Npj Clim. Atmos. Sci.*, 5, 17, <https://doi.org/10.1038/s41612-022-00240-y>,
850 2022.Hodgkins, G. A., Renard, B., Whitfield, P. H., Laaha, G., Stahl, K., Hannaford, J., Burn, D. H., Westra, S., Fleig, A. K.,
851 Araújo Lopes, W. T., Murphy, C., Mediero, L., and Hanel, M.: Climate driven trends in historical extreme low streamflows
852 on four continents, *Water Resour. Res.*, 60, <https://doi.org/10.1029/2022wr034326>, 2024.

853 Holt, A.: New Predictors for Hydrologic Signatures: Wetlands and Geologic Age Across Continental Scales, San Diego State
854 University, United States -- California, 2024.

855 Holt, A. and McMillan, H.: New predictors for hydrologic signatures: Wetlands and geologic age across continental scales,
856 *Hydrol. Process.*, 39, <https://doi.org/10.1002/hyp.70080>, 2025.

857 Horton, J. D., San Juan, C. A., and Stoesser, D. B.: The State Geologic Map Compilation (SGMC) geodatabase of the
858 conterminous United States, <https://doi.org/10.3133/ds1052>, 2017.

859 Hrachowitz, M., Fovet, O., Ruiz, L., Euser, T., Gharari, S., Nijzink, R., Freer, J., Savenije, H. H. G., and Gascuel-Oudou, C.:
860 Process consistency in models: The importance of system signatures, expert knowledge, and process complexity, *Water Resour.*
861 *Res.*, 50, 7445–7469, <https://doi.org/10.1002/2014wr015484>, 2014.

862 Hupp, C. R.: Hydrology, geomorphology and vegetation of Coastal Plain rivers in the south-eastern USA. *Hydrological*
863 *processes*, 14, 2991–3010, 2000.

864 Husic, A.: Game theory for catchment science, ESS Open Archive, <https://doi.org/10.22541/essoar.173924202.27840286/v1>,
865 2025.

866 Husic, A., Hammond, J., Price, A. N., and Roundy, J. K.: Interrogating process deficiencies in large-scale hydrologic models
867 with interpretable machine learning, *Hydrol. Earth Syst. Sci.*, 29, 4457–4472, <https://doi.org/10.5194/hess-29-4457-2025>,
868 2025.

869 Jackisch, C., Angermann, L., Allroggen, N., Sprenger, M., Blume, T., Tronicke, J., and Zehe, E.: Form and function in hillslope
870 hydrology: in situ imaging and characterization of flow-relevant structures, *Hydrol. Earth Syst. Sci.*, 21, 3749–3775, 2017.

871 Janssen, J. and Ameli, A. A.: A hydrologic functional approach for improving large-sample hydrology performance in poorly
872 gauged regions, *Water Resour. Res.*, 57, <https://doi.org/10.1029/2021wr030263>, 2021.

873 Jefferson, A., Grant, G. E., Lewis, S. L., and Lancaster, S. T.: Coevolution of hydrology and topography on a basalt landscape
874 in the Oregon Cascade Range, USA, *Earth Surf. Process.*, <https://doi.org/10.1002/esp.1976>, 2010.

875 Ji, H., Song, Y., Bindas, T., Shen, C., Yang, Y., Pan, M., Liu, J., Rahmani, F., Abbas, A., Beck, H., Lawson, K., and Wada,
876 Y.: Distinct hydrologic response patterns and trends worldwide revealed by physics-embedded learning, *arXiv [physics.geo-*
877 *ph]*, arXiv, 2025.

878 Johnson, J. M., Fang, S., Sankarasubramanian, A., Rad, A. M., Kindl da Cunha, L., Jennings, K. S., Clarke, K. C., Mazrooei,
879 A., and Yeghiazarian, L.: Comprehensive analysis of the NOAA National Water Model: A call for heterogeneous formulations
880 and diagnostic model selection, *J. Geophys. Res.*, 128, <https://doi.org/10.1029/2023jd038534>, 2023.

881 Kavetski, D. and Fenicia, F.: Elements of a flexible approach for conceptual hydrological modeling: 2. Application and
882 experimental insights, *Water Resour. Res.*, 47, <https://doi.org/10.1029/2011wr010748>, 2011.

883 Kennard, M. J., Pusey, B. J., Olden, J. D., Mackay, S. J., Stein, J. L., and Marsh, N.: Classification of natural flow regimes in
884 Australia to support environmental flow management: Classification of natural flow regimes in Australia, *Freshw. Biol.*, 55,
885 171–193, <https://doi.org/10.1111/j.1365-2427.2009.02307.x>, 2010.

886 Kiang, J. E., Stewart, D. W., Archfield, S. A., Osborne, E. B., and Eng, K.: A national streamflow network gap analysis (No.
887 2013-5013), US Geological Survey, 2013.

888 Kirchner, J. W.: Catchments as simple dynamical systems: Catchment characterization, rainfall-runoff modeling, and doing
889 hydrology backward. *Water Resources Research*, 45(2). <https://doi.org/10.1029/2008WR006912>. 2009.

890 Knoben, W. J. M., Woods, R. A., and Freer, J. E.: A quantitative hydrological climate classification evaluated with independent
891 streamflow data, *Water Resour. Res.*, 54, 5088–5109, <https://doi.org/10.1029/2018wr022913>, 2018.

892 Knoben, W. J. M., Freer, J. E., Peel, M. C., Fowler, K. J. A., and Woods, R. A.: A brief analysis of conceptual model structure
893 uncertainty using 36 models and 559 catchments, *Water Resour. Res.*, 56, e2019WR025975,
894 <https://doi.org/10.1029/2019wr025975>, 2020.

895 Krabbenhoft, C. A., Allen, G. H., Lin, P., Godsey, S. E., Allen, D. C., Burrows, R. M., DelVecchia, A. G., Fritz, K. M.,
896 Shanafield, M., Burgin, A. J., Zimmer, M. A., Detry, T., Dodds, W. K., Jones, C. N., Mims, M. C., Franklin, C., Hammond, J.
897 C., Zipper, S., Ward, A. S., Costigan, K. H., Beck, H. E., and Olden, J. D.: Assessing placement bias of the global river gauge
898 network, *Nat. Sustain.*, 5, 586–592, <https://doi.org/10.1038/s41893-022-00873-0>, 2022.

899 Kratzert, F., Nearing, G., Addor, N., Erickson, T., Gauch, M., Gilon, O., Gudmundsson, L., Hassidim, A., Klotz, D., Nevo, S.,
900 Shalev, G., and Matias, Y.: Caravan - A global community dataset for large-sample hydrology, *Sci Data*, 10, 61,
901 <https://doi.org/10.1038/s41597-023-01975-w>, 2023.

902 Kratzert, F., Nearing, G., Addor, N., Erickson, T., Gauch, M., Gilon, O., Gudmundsson, L., Hassidim, A., Klotz, D., Nevo, S.,
903 Shalev, G., and Matias, Y.: Caravan - A global community dataset for large-sample hydrology Version 1.4,
904 <https://doi.org/10.5281/ZENODO.10968468>, 2024.

905 Kuentz, A., Arheimer, B., Hundecha, Y., and Wagener, T.: Understanding hydrologic variability across Europe through
906 catchment classification, *Hydrol. Earth Syst. Sci.*, 21, 2863–2879, 2017.

907 Kuhn, M.: Building predictive models in R using the caret package, *Journal of Statistical Software*, 28, 1–26,
908 <https://doi.org/10.18637/JSS.V028.I05>, 2008.

909 Lane, B. A., Dahlke, H. E., Pasternack, G. B., and Sandoval-Solis, S.: Revealing the Diversity of Natural Hydrologic Regimes
910 in California with Relevance for Environmental Flows Applications, *J. Am. Water Resour. Assoc.*, 53, 411–430,
911 <https://doi.org/10.1111/1752-1688.12504>, 2017.

912 Lane, C. R. and D’Amico, E.: Identification of putative geographically isolated wetlands of the conterminous United States, *J.*
913 *Am. Water Resour. Assoc.*, 52, 705–722, <https://doi.org/10.1111/1752-1688.12421>, 2016.

914 Lapedes, D. A., Zipper, S., and Hammond, J. C.: Identifying hydrologic signatures associated with streamflow depletion caused
915 by groundwater pumping, *Hydrol. Process.*, 37, <https://doi.org/10.1002/hyp.14877>, 2023.

916 Lee, D., Ward, P., and Block, P.: Defining high-flow seasons using temporal streamflow patterns from a global model, *Hydrol.*
917 *Earth Syst. Sci.*, 19, 4689–4705, <https://doi.org/10.5194/hess-19-4689-2015>, 2015.

918 Linke, S., Lehner, B., Ouellet Dallaire, C., Ariwi, J., Grill, G., Anand, M., Beames, P., Burchard-Levine, V., Maxwell, S.,
919 Moidu, H., Tan, F., and Thieme, M.: Global hydro-environmental sub-basin and river reach characteristics at high spatial
920 resolution, *Sci Data*, 6, 283, <https://doi.org/10.1038/s41597-019-0300-6>, 2019.

921 Lins, H. F.: Regional streamflow regimes and hydroclimatology of the United States, *Water Resour. Res.*, 33, 1655–1667,
922 <https://doi.org/10.1029/97WR00615>, 1997.

923 Lohse, K. A. and Dietrich, W. E.: Contrasting effects of soil development on hydrological properties and flow paths, *Water*
924 *Resour. Res.*, 41, <https://doi.org/10.1029/2004wr003403>, 2005.

925 Lundberg, S. and Lee, S.-I.: A unified approach to interpreting model predictions, *arXiv [cs.AI]*, arXiv, 2017.

926 Lundberg, S. M., Erion, G. G., and Lee, S.-I.: Consistent individualized feature attribution for tree ensembles, *arXiv [cs.LG]*,
927 arXiv, 2018.

928 Markstrom, S. L., Hay, L. E., and Clark, M. P.: Towards simplification of hydrologic modeling: identification of dominant
929 processes, *Hydrol. Earth Syst. Sci.*, 20, 4655–4671, <https://doi.org/10.5194/hess-20-4655-2016>, 2016.

930 Mazvimavi, D., Meijerink, A. M. J., Savenije, H. H. G., and Stein, A.: Prediction of flow characteristics using multiple
931 regression and neural networks: A case study in Zimbabwe, *Phys. Chem. Earth* (2002), 30, 639–647,
932 <https://doi.org/10.1016/j.pce.2005.08.003>, 2005.

933 McGrath, G. S., Hinz, C., and Sivapalan, M.: Temporal dynamics of hydrological threshold events, *Hydrol. Earth Syst. Sci.*,
934 11, 923–938, <https://doi.org/10.5194/hess-11-923-2007>, 2007.

935 McMillan, H.: Linking hydrologic signatures to hydrologic processes: A Review, *Hydrol. Process.*, 34, 1393–1409,
936 <https://doi.org/10.1002/hyp.13632>, 2020.

937 McMillan, H., Gueguen, M., Grimon, E., Woods, R., Clark, M., and Rupp, D. E.: Spatial variability of hydrological processes
938 and model structure diagnostics in a 50 km² catchment, *Hydrol. Process.*, 28, 4896–4913, <https://doi.org/10.1002/hyp.9988>,
939 2014.

940 McMillan, H., Westerberg, I., and Branger, F.: Five guidelines for selecting hydrological signatures, *Hydrol. Process.*, 31,
941 4757–4761, <https://doi.org/10.1002/hyp.11300>, 2017.

942 McMillan, H., Araki, R., Bolotin, L., Kim, D.-H., Coxon, G., Clark, M., and Seibert, J.: Global patterns in observed hydrologic
943 processes, *Nat Water*, <https://doi.org/10.1038/s44221-025-00407-w>, 2025.

944 McMillan, H. K.: A review of hydrologic signatures and their applications, *WIREs Water*, 8, <https://doi.org/10.1002/wat2.1499>,
945 2021.

946 McMillan, H. K., Gnann, S. J., and Araki, R.: Large scale evaluation of relationships between hydrologic signatures and
947 processes, *Water Resour. Res.*, 58, <https://doi.org/10.1029/2021wr031751>, 2022.

948 McMillan, H., Coxon, G., Araki, R., Salwey, S., Kelleher, C., Zheng, Y., Knoben, W., Gnann, S., Seibert, J., and Bolotin, L.:
949 When good signatures go bad: Applying hydrologic signatures in large sample studies, *Hydrol. Process.*, 37,
950 <https://doi.org/10.1002/hyp.14987>, 2023.

951 McMillan, H. K., Coxon, G., Araki, R., Salwey, S., Kelleher, C., Zheng, Y., Knoben, W., Gnann, S., Seibert, J., and Bolotin,
952 L.: When good signatures go bad: Applying hydrologic signatures in large sample studies, *Hydrol. Process.*, 37,
953 <https://doi.org/10.1002/hyp.14987>, 2023.

954 Miller, D. A. and White, R. A.: A conterminous United States multilayer soil characteristics dataset for regional climate and
955 hydrology modeling, *Earth Interact.*, 2, 1–26, [https://doi.org/10.1175/1087-3562\(1998\)002<0001:acusms>2.3.co;2](https://doi.org/10.1175/1087-3562(1998)002<0001:acusms>2.3.co;2), 1998.

956 Miller, J. A.: Ground water atlas of the United States: Introduction and national summary (No. 730-A), A1–A15, 1999.

957 Molnar, C., Bischl, B., and Casalicchio, G.: iml: An R package for Interpretable Machine Learning,
958 <https://doi.org/10.21105/joss.00786>, 2018.

959 Miller, D. A. and White, R. A.: A conterminous United States multilayer soil characteristics dataset for regional climate and
960 hydrology modeling, *Earth Interact.*, 2, 1–26, [https://doi.org/10.1175/1087-3562\(1998\)002%3C0001:acusms%3E2.3.co;2](https://doi.org/10.1175/1087-3562(1998)002%3C0001:acusms%3E2.3.co;2),
961 1998.

962 Mosley, M. P.: Delimitation of New Zealand hydrologic regions, *J. Hydrol. (Amst.)*, 49, 173–192,
963 [https://doi.org/10.1016/0022-1694\(81\)90211-0](https://doi.org/10.1016/0022-1694(81)90211-0), 1981.

964 Muñoz Sabater, J.: ERA5-Land monthly averaged data from 1950 to present, <https://doi.org/10.24381/CDS.68D2BB30>, 2019.

965 Neff, B. P., Day, S. M., Piggott, A. R., and Fuller, L. M.: Base flow in the Great Lakes Basin,
966 <https://doi.org/10.3133/sir20055217>, 2005.

967 Noguchi, S., Nik, A. R., Yusop, Z., Tani, M., and Sammori, T.: Rainfall-runoff responses and roles of soil moisture variations
968 to the response in tropical Rain Forest, Bukit Tarek, peninsular Malaysia, *J. Forest Res.*, 2, 125–132,
969 <https://doi.org/10.1007/bf02348209>, 1997.

970 Ogden, F., Avant, B., Bartel, R., Blodgett, D., Clark, E., Coon, E., Cosgrove, B., Cui, S., Kindl da Cunha, L., Farthing, M.,
971 Flowers, T., Frame, J., Frazier, N., Graziano, T., Gutenson, J., Johnson, D., McDaniel, R., Moulton, J., Loney, D., Peckham,
972 S., Mattern, D., Jennings, K., Williamson, M., Savant, G., Tubbs, C., Garrett, J., Wood, A., and Johnson, J.: The Next
973 Generation Water Resources Modeling Framework: Open Source, Standards Based, Community Accessible, Model
974 Interoperability for Large Scale Water Prediction, AGU Fall Meeting Abstracts, New Orleans, LA, 2021, H43D–01, 2021.

975 Omernik, J. M.: Ecoregions of the conterminous United States, *Ann. Assoc. Am. Geogr.*, 77, 118–125, 1987.

976 Omernik, J. M.: Perspectives on the nature and definition of ecological regions, *Environ. Manage.*, 34 Suppl 1, S27–38,
977 <https://doi.org/10.1007/s00267-003-5197-2>, 2004.

978 Oswald, C. J., Kelleher, C., Ledford, S. H., Hopkins, K. G., Sytsma, A., Tetzlaff, D., Toran, L., and Voter, C.: Integrating
979 urban water fluxes and moving beyond impervious surface cover: A review, *J. Hydrol. (Amst.)*, 618, 129188,
980 <https://doi.org/10.1016/j.jhydrol.2023.129188>, 2023.

981 Oudin, L., Andréassian, V., Perrin, C., Michel, C., and Le Moine, N.: Spatial proximity, physical similarity, regression and
982 ungaged catchments: A comparison of regionalization approaches based on 913 French catchments, *Water Resources Research*,
983 44, <https://doi.org/10.1029/2007WR006240>, 2008.

984 Paola, C., Foufoula-Georgiou, E., Dietrich, W. E., Hondzo, M., Mohrig, D., Parker, G., Power, M. E., Rodriguez-Iturbe, I.,
985 Veldkamp, T. I. E., Wada, Y., Aerts, J. C. J. H., Döll, P., Gosling, S. N., Liu, J., Masaki, Y., Oki, T., Ostberg, S., Pokhrel, Y.,
986 Satoh, Y., Kim, H., and Ward, P. J.: Water scarcity hotspots travel downstream due to human interventions in the 20th and
987 21st century, *Nat. Commun.*, 8, 15697, <https://doi.org/10.1038/ncomms15697>, 2017.

988 Vogel, R. M., Member, J., and Asce, N. M.: Flow-duration curves. I: New interpretation and confidence intervals, [https://bpb-](https://bpb-us-e1.wpmucdn.com/sites.tufts.edu/dist/a/4406/files/2019/04/flowDuration1.pdf)
989 [us-e1.wpmucdn.com/sites.tufts.edu/dist/a/4406/files/2019/04/flowDuration1.pdf](https://bpb-us-e1.wpmucdn.com/sites.tufts.edu/dist/a/4406/files/2019/04/flowDuration1.pdf).

990 Voller, V., and Wilcock, P.: Toward a unified science of the Earth’s surface: Opportunities for synthesis among hydrology,
991 geomorphology, geochemistry, and ecology, *Water Resour. Res.*, 42, <https://doi.org/10.1029/2005wr004336>, 2006.

992 Payn, R. A., Gooseff, M. N., and McGlynn, B. L.: Exploring changes in the spatial distribution of stream baseflow generation
993 during a seasonal recession, <https://doi.org/10.1029/2011WR011552>, 2012.

994 Pechlivanidis, I. G. and Arheimer, B.: Large-scale hydrological modelling by using modified PUB recommendations: the
995 India-HYPE case, *Hydrol. Earth Syst. Sci.*, 19, 4559–4579, <https://doi.org/10.5194/hess-19-4559-2015>, 2015.

996 Pedregosa, F., Varoquaux, G., Gramfort, A., Michel, V., Thirion, B., Grisel, O., Blondel, M., Prettenhofer, P., Weiss, R.,
997 Dubourg, V., Vanderplas, J., Passos, A., Cournapeau, D., Brucher, M., Perrot, M., and Duchesnay, E.: Scikit-learn: Machine
998 Learning in Python, *Journal of Machine Learning Research*, 12, 2825–2830, 2011.

999 Penna, D.: A recipe for why and how to set up and sustain an experimental catchment, *Hydrol. Process.*, 38,
1000 <https://doi.org/10.1002/hyp.15163>, 2024.

1001 Peters, N. E. and Aulenbach, B. T.: Water storage at the Panola mountain research watershed, Georgia, USA: Water storage
1002 at pmrw, *Hydrol. Process.*, 25, 3878–3889, <https://doi.org/10.1002/hyp.8334>, 2011.

1003 Pfister, L., Martínez-Carreras, N., Hissler, C., Klaus, J., Carrer, G. E., Stewart, M. K., and McDonnell, J. J.: Bedrock geology
1004 controls on catchment storage, mixing, and release: A comparative analysis of 16 nested catchments, *Hydrological Processes*,
1005 31, 1828–1845, <https://doi.org/10.1002/hyp.11134>, 2017.

1006 Prieto, C., Kavetski, D., Le Vine, N., Álvarez, C., and Medina, R.: Identification of dominant hydrological mechanisms using
1007 Bayesian inference, multiple statistical hypothesis testing, and flexible models, *Water Resour. Res.*, 57,
1008 <https://doi.org/10.1029/2020wr028338>, 2021.

1009 Qi, S. L. and Mason, C. A.: Data used to prioritize the selection of river basins for intensive monitoring and assessment by the
1010 U.S. Geological Survey, <https://doi.org/10.5066/P98194QR>, 2023.

1011 R Core Team (2024). R: A Language and Environment for Statistical Computing. R Foundation for Statistical Computing,
1012 Vienna, Austria. <https://www.R-project.org/>.

1013 Reinecke, R., Stein, L., Gnann, S., Andersson, J. C. M., Arheimer, B., Bierkens, M., Bonetti, S., Güntner, Kollet, S., Mishra,
1014 S., Moosdorf, N., Nazari, S., Pokhrel, Y., Prudhomme, C., Schewe, J., Shen, C., and Wagener, T.: Uncertainties guide global
1015 water model advancement, *WIREs Water*, 12, <https://doi.org/10.1002/wat2.70025>, 2025.

1016 Renken, R. A.: Ground Water Atlas of the United States: Segment 5, Arkansas, Louisiana, Mississippi, *Hydrologic Atlas 730*,
1017 28p., U.S. Geological Survey, <https://doi.org/10.3133/ha730F>, 1998.

1018 Robert Maier, H., Rosa Taghikhah, F., Nabavi, E., Razavi, S., Gupta, H., Wu, W., Radford, D. A. G., and Huang, J.: How
1019 much X is in XAI: Responsible use of “Explainable” artificial intelligence in hydrology and water resources, *J. Hydrol. X*, 25,
1020 100185, <https://doi.org/10.1016/j.hydroa.2024.100185>, 2024.

1021 Rudlang, J. M., do Nascimento, T. V. M., van der Ent, R., Fenicia, F., and Hrachowitz, M.: Climate and landscape jointly
1022 control Europe's hydrology, *EGUsphere* [preprint], <https://doi.org/10.5194/egusphere-2025-6372>, 2025.

1023 Safeeq, M. and Hunsaker, C. T.: Characterizing runoff and water yield for headwater catchments in the southern Sierra Nevada,
1024 *J. Am. Water Resour. Assoc.*, 52, 1327–1346, <https://doi.org/10.1111/1752-1688.12457>, 2016.

1025 Safeeq, M., Grant, G. E., Lewis, S. L., and Tague, C. L.: Coupling snowpack and groundwater dynamics to interpret historical
1026 streamflow trends in the western United States: COUPLING SNOWPACK AND GROUNDWATER DYNAMICS TO
1027 INTERPRET STREAMFLOW, *Hydrol. Process.*, 27, 655–668, <https://doi.org/10.1002/hyp.9628>, 2013.

1028 Santhi, C., Allen, P. M., Muttiah, R. S., Arnold, J. G., and Tuppap, P.: Regional estimation of base flow for the conterminous
1029 United States by hydrologic landscape regions, *J. Hydrol. (Amst.)*, 351, 139–153,
1030 <https://doi.org/10.1016/j.jhydrol.2007.12.018>, 2008.

1031 Sauquet, E., Shanafield, M., Hammond, J. C., Sefton, C., Leigh, C., and Datry, T.: Classification and trends in intermittent
1032 river flow regimes in Australia, northwestern Europe and USA: A global perspective, *J. Hydrol. (Amst.)*, 597, 126170,
1033 <https://doi.org/10.1016/j.jhydrol.2021.126170>, 2021.

1034 Seaber, P. R., Kapinos, F. P., and Knapp, G. L.: Hydrologic unit maps, US Geological Survey, <https://doi.org/10.3133/wsp2294>,
1035 1987.

1036 Sebestyen, S. D., Shanley, J. B., Blume, T., Duncan, J. M., Jones, J., Segura, C., and Mast, M. A.: Introduction to the special
1037 issue on research and observatory catchments, *Hydrol. Process.*, 39, <https://doi.org/10.1002/hyp.70069>, 2025.

1038 Shalev, G. and Kratzert, F.: Caravan MultiMet: Extending Caravan with multiple weather nowcasts and forecasts, arXiv
1039 [cs.LG], arXiv, 2024.

1040 Shanley, J. B., Sebestyen, S. D., McDonnell, J. J., McGlynn, B. L., and Dunne, T.: Water’s Way at Sleepers River watershed
1041 – revisiting flow generation in a post-glacial landscape, Vermont USA, *Hydrol. Process.*, 29, 3447–3459,
1042 <https://doi.org/10.1002/hyp.10377>, 2015.

1043 Shapley, L. S.: 17. A Value for n-Person Games, in: *Contributions to the Theory of Games (AM-28)*, Volume II, edited by:
1044 Kuhn, H. W. and Tucker, A. W., Princeton University Press, Princeton, 307–318, <https://doi.org/10.1515/9781400881970-018>,
1045 1953.

1046 Shaw, S. B. and Riha, S. J.: Examining individual recession events instead of a data cloud: Using a modified interpretation of
1047 $dQ/dt-Q$ streamflow recession in glaciated watersheds to better inform models of low flow, *J. Hydrol. (Amst.)*, 434-435, 46–
1048 54, <https://doi.org/10.1016/j.jhydrol.2012.02.034>, 2012.

1049 Shrestha, D., Howard, D., and Benedict, T. D.: Moderate Resolution Imaging Spectroradiometer (MODIS) irrigated
1050 Agriculture datasets for the conterminous United States (MirAD-US), <https://doi.org/10.5066/P9NA3EO8>, 2019.

1051 Sivapalan, M.: Pattern, process and function: Elements of a unified theory of hydrology at the catchment scale, in:
1052 *Encyclopedia of Hydrological Sciences*, Wiley, Chichester, UK, <https://doi.org/10.1002/0470848944.hsa012>, 2005.

1053 Web Soil Survey: <http://websoilsurvey.nrcs.usda.gov/>, last access: 11 May 2025.

1054 Spieler, D., Mai, J., Craig, J. R., Tolson, B. A., and Schütze, N.: Automatic model structure identification for conceptual
1055 hydrologic models, *Water Resour. Res.*, 56, <https://doi.org/10.1029/2019wr027009>, 2020.

1056 Stein, L., Clark, M. P., Knoben, W. J., Pianosi, F., & Woods, R. A.: How do climate and catchment attributes influence flood
1057 generating processes? A large-sample study for 671 catchments across the contiguous USA. *Water Resources Research*, 57(4),
1058 e2020WR028300. <https://doi.org/10.1029/2020WR028300>, 2021.

1059 Stets, E. G., Archer, A. A., Degnan, J. R., Erickson, M. L., Gorski, G., Medalie, L., and Scholl, M. A.: The National integrated
1060 water availability assessment, 2025.

1061 Tague, C. and Grant, G. E.: A geological framework for interpreting the low-flow regimes of Cascade streams, Willamette
1062 River Basin, Oregon: GEOLOGICAL FRAMEWORK FOR LOW-FLOW REGIMES, *Water Resour. Res.*, 40,
1063 <https://doi.org/10.1029/2003wr002629>, 2004.

1064 Tague, C. and Grant, G. E.: Groundwater dynamics mediate low-flow response to climate warming in snow-dominated alpine
1065 regions, *Water Resources Research*, 45, 2009.

1066 Tallaksen, L. M.: A review of baseflow recession analysis, *J. Hydrol.*, 165, 349–370, [https://doi.org/10.1016/0022-1694\(94\)02540-R](https://doi.org/10.1016/0022-1694(94)02540-R), 1995.

1068 Tarasova, L., Gnann, S., Yang, S., Hartmann, A., and Wagener, T.: Catchment characterization: Current descriptors,
1069 knowledge gaps and future opportunities, *Earth Sci. Rev.*, 252, 104739, <https://doi.org/10.1016/j.earscirev.2024.104739>, 2023.

1070 Thompson, J. M., Hathaway, J. M., Perfect, E., and Schwartz, J. S.: The effect of stormwater infiltration and surrounding built
1071 infrastructure on local groundwater dynamics: a case study for regenerative stormwater conveyances, *Sustain. Resilient*
1072 *Infrastruct.*, 1–11, <https://doi.org/10.1080/23789689.2020.1772636>, 2020.

1073 Trancoso, R., Phinn, S., McVicar, T., Larsen, J., and McAlpine, C.: Regional variation in streamflow drivers across a
1074 continental climatic gradient, *Ecohydrology*, 10, e1816, <https://doi.org/10.1002/eco.1816>, 2017.

1075 Tran, V. N.: CAMELSH: A large-sample hourly hydrometeorological dataset and attributes at watershed-scale for contiguous
1076 United States, <https://doi.org/10.5281/ZENODO.15070091>, 2025.

1077 Tran, V. N., Xu, D., Van Nguyen, T., Kim, T., and Ivanov, V. Y.: CAMELSH: A large-sample hourly hydrometeorological
1078 dataset and attributes at watershed-scale for CONUS, *Sci. Data*, 12, 1307, <https://doi.org/10.1038/s41597-025-05612-6>, 2025.

1079 Turner, S., Hannaford, J., Barker, L. J., Suman, G., Killeen, A., Armitage, R., Chan, W., Davies, H., Griffin, A., Kumar, A.,
1080 Dixon, H., Albuquerque, M. T. D., Almeida Ribeiro, N., Alvarez-Garreton, C., Amoussou, E., Arheimer, B., Asano, Y.,
1081 Berezowski, T., Bodian, A., Boutaghane, H., Capell, R., Dakhaoui, H., Daňhelka, J., Do, H. X., Ekkawatpanit, C., El Khalki,
1082 E. M., Fleig, A. K., Fonseca, R., Giraldo-Osorio, J. D., Goula, A. B. T., Hanel, M., Horton, S., Kan, C., Kingston, D. G., Laaha,
1083 G., Laugesen, R., Lopes, W., Mager, S., Rachdane, M., Markonis, Y., Medeiro, L., Midgley, G., Murphy, C., O'Connor, P.,
1084 Pedersen, A. I., Pham, H. T., Piniewski, M., Renard, B., Saidi, M. E., Schmocker-Fackel, P., Stahl, K., Thyer, M., Toucher,
1085 M., Trambly, Y., Uusikivi, J., Venegas-Cordero, N., Visessri, S., Watson, A., Westra, S., and Whitfield, P. H.: ROBIN:
1086 Reference observatory of basins for international hydrological climate change detection, *Sci. Data*, 12, 654,
1087 <https://doi.org/10.1038/s41597-025-04907-y>, 2025.

1088 UKIH: UK Institute of Hydrology (Great Britain), Low Flow Studies Reports, Institute of Hydrology, 1980.

1089 United States Department of Agriculture, Soil Survey Staff, and Natural Resources Conservation: U.S. General Soil Map
1090 (STATSGO): Web soil survey, 2008.

1091 United States Geological Survey: Protected Areas Database of the United States (PAD-US) 4,
1092 <https://doi.org/10.5066/P96WBCHS>, 2024.

1093 U.S. Environmental Protection Agency: National Hydrography Dataset Plus (NHDPlus): USEPA; USGS; and Horizon
1094 Systems Corporation, 2008.

1095 U.S. Geological Survey: USGS Water Data for the Nation: U.S. Geological Survey National Water Information System
1096 Database, <https://doi.org/10.5066/F7P55KJN>, 2025.

1097 Valeron, B. and Meixner, T.: Overland flow generation in chaparral ecosystems: temporal and spatial variability, *Hydrol.*
1098 *Process.*, 24, 65–75, <https://doi.org/10.1002/hyp.7455>, 2010.

1099 Van Metre, P. C., Qi, S., Deacon, J., Dieter, C., Driscoll, J. M., Fienen, M., Kenney, T., Lambert, P., Lesmes, D., Mason, C.
1100 A., Mueller-Solger, A., Musgrove, M., Painter, J., Rosenberry, D., Sprague, L., Tesoriero, A. J., Windham-Myers, L., and
1101 Wolock, D.: Prioritizing river basins for intensive monitoring and assessment by the US Geological Survey, *Environ. Monit.*
1102 *Assess.*, 192, 458, <https://doi.org/10.1007/s10661-020-08403-1>, 2020.

1103 Westerberg, I. K., Wagener, T., Coxon, G., McMillan, H. K., Castellarin, A., Montanari, A., and Freer, J.: Uncertainty in
1104 hydrological signatures for gauged and ungauged catchments, *Water Resources Research*, 52, 1847–1865,
1105 <https://doi.org/10.1002/2015WR017635>, 2016.

1106 Wieczorek, M. E. and LaMotte, A. E.: Attributes for NHDPlus Catchments (Version 1.1) for the Conterminous United States:
1107 Average Saturation Excess-Overland Flow, 2002: U.S. Geological Survey data release, 2010.

1108 Wieczorek, M. E., Hafen, K. C., and Staub, L. E.: Data-Driven Drought Prediction Project model inputs for Upper and Lower
1109 Colorado portions of the national hydrologic Geo-spatial fabric version 1.1 and select U.S. geological Survey streamgage basins
1110 (ver. 2.0, July 2025), <https://doi.org/10.5066/P98IG8LO>, 2023.

1111 Willard, J. D., Ciulla, F., Weierbach, H., Kumar, V., and Varadharajan, C.: Evaluating deep learning approaches for predictions
1112 in unmonitored basins with continental-scale stream temperature models, *arXiv [cs.LG]*, arXiv, 2024.

1113 Williams, P. W. and Ford, D. C.: Global distribution of carbonate rocks, *Zeitschrift für Geomorphologie Suppl*, 147, 1–2, 2006.

1114 Wilson, C. G., Papanicolaou, A. N. T., and Denn, K. D.: Partitioning fine sediment loads in a headwater system with intensive
1115 agriculture, *J. Soils Sediments*, 12, 966–981, <https://doi.org/10.1007/s11368-012-0504-2>, 2012.

1116 Winter, T. C.: The Concept of Hydrologic Landscapes, *JAWRA Journal of the American Water Resources Association*, 37,
1117 335–349, <https://doi.org/10.1111/j.1752-1688.2001.tb00973.x>, 2001.

1118 Wlostowski, A. N., Molotch, N., Anderson, S. P., Brantley, S. L., Chorover, J., Dralle, D., Kumar, P., Li, L., Lohse, K. A.,
1119 Mallard, J. M., McIntosh, J. C., Murphy, S. F., Parrish, E., Safeeq, M., Seyfried, M., Shi, Y., and Harman, C.: Signatures of
1120 Hydrologic Function Across the Critical Zone Observatory Network, *Water Resour. Res.*, 57, e2019WR026635,
1121 <https://doi.org/10.1029/2019wr026635>, 2021.

1122 Wolock, D. M.: Hydrologic landscape regions of the United States, US Geological Service, 2003a.

1123 Wolock, D. M.: Infiltration-excess overland flow estimated by TOPMODEL for the conterminous United States (No. 2003-
1124 310), US Geological Survey., 2003b.

1125 Wu, S., Zhao, J., Wang, H., and Sivapalan, M.: Regional patterns and physical controls of streamflow generation across the
1126 conterminous United States, *Water Resour. Res.*, 57, e2020WR028086, <https://doi.org/10.1029/2020wr028086>, 2021.

1127 Xia, Y., Mitchell, K., Ek, M., Sheffield, J., Cosgrove, B., Wood, E., Luo, L., Alonge, C., Wei, H., Meng, J., Livneh, B.,
1128 Lettenmaier, D., Koren, V., Duan, Q., Mo, K., Fan, Y., and Mocko, D.: Continental-scale water and energy flux analysis and

1129 validation for the North American Land Data Assimilation System project phase 2 (NLDAS-2): 1. Intercomparison and
1130 application of model products, *J. Geophys. Res. D: Atmos.*, 117, <https://doi.org/10.1029/2011JD016048>, 2012.

1131 Xie, J., Liu, X., Jasechko, S., Berghuijs, W. R., Wang, K., Liu, C., Reichstein, M., Jung, M., and Koirala, S.: Majority of global
1132 river flow sustained by groundwater, *Nat. Geosci.*, 17, 770–777, <https://doi.org/10.1038/s41561-024-01483-5>, 2024.

1133 Yang, L., Jin, S., Danielson, P., Homer, C., Gass, L., Bender, S. M., Case, A., Costello, C., Dewitz, J., Fry, J., Funk, M.,
1134 Granneman, B., Liknes, G. C., Rigge, M., and Xian, G.: A new generation of the United States National Land Cover Database:
1135 Requirements, research priorities, design, and implementation strategies, *ISPRS J. Photogramm. Remote Sens.*, 146, 108–123,
1136 <https://doi.org/10.1016/j.isprsjprs.2018.09.006>, 2018.

1137 Yilmaz, K. K., Gupta, H. V., and Wagener, T.: A process-based diagnostic approach to model evaluation: Application to the
1138 NWS distributed hydrologic model, *Water Resour. Res.*, 44, <https://doi.org/10.1029/2007wr006716>, 2008.

1139 Zimmer, M. A. and Gannon, J. P.: Run-off processes from mountains to foothills: The role of soil stratigraphy and structure
1140 in influencing run-off characteristics across high to low relief landscapes, *Hydrol. Process.*, 32, 1546–1560,
1141 <https://doi.org/10.1002/hyp.11488>, 2018.

1142 Zipper, S. C., Hammond, J. C., Shanafield, M., Zimmer, M., Datry, T., Jones, C. N., Kaiser, K. E., Godsey, S. E., Burrows, R.
1143 M., Blaszcak, J. R., Busch, M. H., Price, A. N., Boersma, K. S., Ward, A. S., Costigan, K., Allen, G. H., Krabbenhoft, C. A.,
1144 Dodds, W. K., Mims, M. C., Olden, J. D., Kampf, S. K., Burgin, A. J., and Allen, D. C.: Pervasive changes in stream
1145 intermittency across the United States, *Environ. Res. Lett.*, 16, 084033, <https://doi.org/10.1088/1748-9326/ac14ec>, 2021.